2018-04-01

Using Collapsible Systems to Mitigate Buckling in Thin Flexible Instruments in Robotic Surgery

Brandon Scott Sargent
Brigham Young University

Using Collapsible Systems to Mitigate Buckling in Thin Flexible Instruments in Robotic Surgery

Brandon Scott Sargent

A thesis submitted to the faculty of
Brigham Young University
in partial fulfillment of the requirements for the degree of

Master of Science

Brian D. Jensen, Chair
Larry L Howell
Spencer P. Magleby

Department of Mechanical Engineering

Brigham Young University

ABSTRACT

Using Collapsible Systems to Mitigate Buckling
in Thin Flexible Instruments in Robotic Surgery

Brandon Scott Sargent
Department of Mechanical Engineering, BYU
Master of Science

Robotic surgery procedures may include long, thin flexible instruments that are inserted by the robot into the patient. As the robot inserts these devices, due to their geometry, they are prone to buckling failure. To mitigate buckling failure, a support system is needed on the robot. This system supports the device but also adapts to the varying ex vivo length of the device as it is inserted. This work presents four collapsible support systems designed to mitigate buckling failure of long, thin instruments while accounting for changing length.

The Ori-Guide is an origami-inspired system that has enabled a part reduction from traditional rigid systems with over 70 parts to 3 parts. This system was enabled through the development of a novel origami pattern that integrates both actuation and support into the same pattern. This system was made from PET and performed as well as a rigid system. The PET used in the Ori-Guide was thermo-processed to hold a folded shape. The heat treatment put the Ori-Guide into tension and enabled a stiffer support system. Work was done to investigate the effect of thermo-processing on PET films used in origami-inspired engineering applications. It was discovered that there is a strong correlation between crystallization and the stiffness of a crease in the polymer film.

The Zipper-Tube Reinforcement (ZTR) was developed to provide constant support along the entire length of the device, something that no other support device provides. This enables higher loads on the device and thinner and more flexible devices. It was developed as a tube that envelopes the device and zips to provide a tube to support the device then unzips to lay flat rolled about a mandrel for storage.

The Wires in Tension concept was developed by focusing on adding tension to the support system. It provided support to the device but required high levels of force on the robot arm so the Orthogonal Beams was developed. The Orthogonal Beams employs geometry as the primary support rather than tension and therefore could provide higher support with less force on the robot.

These systems all proved effective ways to support flexible devices. The concepts could also find application in other fields. The merits of each system are discussed in detail, including a discussion on other possible applications.

Keywords: compliant mechanisms, buckling, lateral stiffness, robotic surgery, PET, origami

ACKNOWLEDGMENTS

This research was funded through a grant from Intuitive Surgical, Inc. I would like to offer special thanks to David Bailey and the others at Intuitive Surgical for their guidance, direction, and expertise. Their contribution enabled the work presented here.

I would like to express gratitude for the tutelage of my committee, namely my advisor, Dr. Brian Jensen, and Drs. Larry Howell and Spencer Magleby. Their guidance has been crucial to not only the projects and concepts developed and presented in this work, but also to my personal development.

The Compliant Mechanisms Research Group, of which I have been a part during this research, have provided support and intuition as the project began, developed, and came to a close. Collaboration with my coworkers in the lab provided important insight as we grappled with difficult problems. A special thanks to those members of my team who gave many hours to the development of the concepts, help with prototyping and testing, and writing. I am so grateful for all those I have worked with and developed friendships with through the course of this work.

I want to give special thanks to my family, their never ending support and encouragement and rearing me and starting me on the path that would get me to this point. Their love is one of my greatest motivations. I am also so grateful for my friends who have been there for me in the lab and those who have helped, supported, and loved me in my personal life. Their friendships have provided needed rejuvenation and strength to focus on my work when in the lab.

Most of all I want to express gratitude and acknowledge the hand of the Lord Jesus Christ in supporting me, inspiring me, and giving me the strength and knowledge that I needed for the tasks required. All knowledge comes from Him and without Him this project would surely have never come to fruition.

TABLE OF CONTENTS

LIST OF TABLES

LIST OF FIGURES

CHAPTER 1. INTRODUCTION

Innovation in surgical robotics has provided surgeons with new methods for accessing areas inside the patient through minimally invasive approaches. Minimally invasive surgery (MIS) techniques are becoming more desirable due to the reduction in trauma to the patient and decreased recovery time. For medical robotics designed for MIS approaches, a variety of devices have been designed or adapted for the small incisions used in MIS. Two primary devices used in a medical robot system are an endoscope and a catheter. An endoscope is typically used to provide a live camera feed of the work area or to observe an area of the body for diagnosis without requiring open, highly-invasive approaches. A catheter is a flexible cylindrical tube fed into the body through the circulatory, respiratory, or digestive systems. The catheter is then used to deploy a device, take a sample, or deliver a fluid into the body.

For the use of both catheters and endoscopes, the device needs to be long, thin, and flexible to access the largest range of areas in the body. Smaller diameter devices also cause less trauma on the patient, both in reducing rubbing contact with the skin and reducing incision size when an incision is required for insertion. Because both length and a small diameter are desired, these instruments are prone to buckling when loaded in compression. Inside the body, the surrounding tissue adds the required support to avoid buckling internally. However, outside the body the instrument needs to be advanced into the body while being supported against buckling and protected from kinking or bending that could damage the instrument. During robotic surgery, the robot would be required to support the instrument while still applying a compressive load to insert it.

In addressing this need, the focus of this research is to develop an understanding of principles that can be applied in the development of mechanical support systems. These systems need to be capable of compressing and extending to the same range of the insertion stroke of the robot to adapt to the varying out-of-body length of the device. Therefore the principles investigated must be able to be applied in varying length systems. As further understanding is developed, support

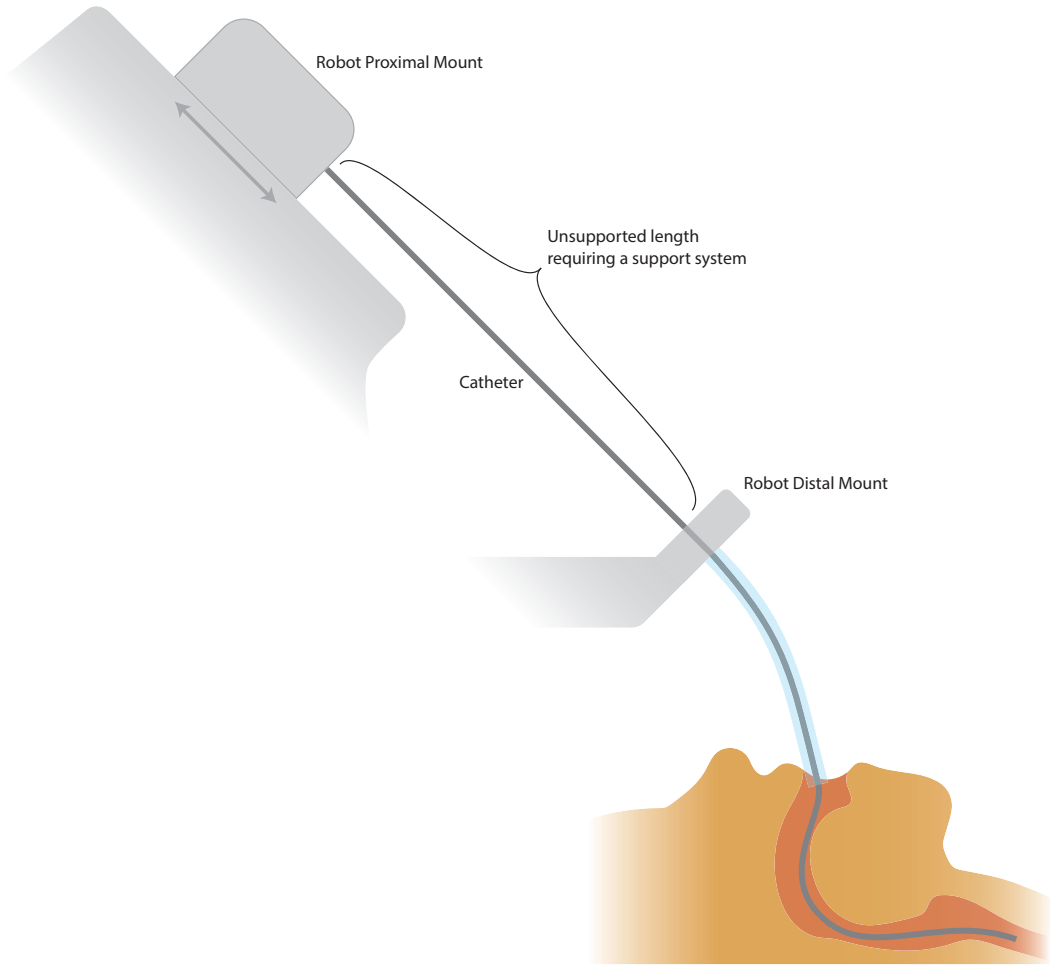

Figure 1.1: An example of a robot system inserting a catheter through the airways for a lung biopsy. The robot proximal mount pushes the catheter axially toward the distal mount to advance the catheter into the body. The space between the mounts is where the support system is needed to prevent buckling.

systems will be created that apply these principles to demonstrate the application and effectiveness of the principles in mechanical support systems for thin, flexible devices.

An example of the use of thin, flexible devices is a catheters used in surgical robotics in lung cancer diagnosis. In the United States, lung cancer is the second most common cancer in men and women and the leading cause of cancer related death, projected to account for 25.3% of cancer related deaths in the US in 2018. Survival rates for those diagnosed with lung cancer depends on when it is diagnosed [1].

One of the primary ways for diagnosing and staging lung cancer is through a biopsy of the tumor. The biopsy is taken by inserting a needle into the tumor and retrieving a core sample or using fine needle aspiration to withdraw smaller segments of tissue. A common approach to needle biopsies is through the skin and into the lung. This requires the needle to puncture the lung and air may leak from the lungs into the chest cavity and can cause the lung to collapse [2].

A flexible catheter could be inserted by a robot into the lungs through the mouth which would move through the airways until it could find the suspected cancerous site and take a biopsy as shown in Figure 1.1. This solution is avoids the risk of the lung collapsing. A limiting factor in this approach is the deep areas of the lung are difficult to access due to the decreasing diameters of the branching airways in the lung. The smaller the catheter, the more access the surgeon has to the deeper areas of the lung. Lung biopsies are just one example of how smaller devices enable greater access for surgical staff. Other areas could include cardiovascular and gastroentrological procedures and pediatric surgeries to name a few.

1.1 Background

For long, thin members under compressive loading, buckling is one of the most common reasons for failure. Buckling is a compressive loading phenomenon and is well studied and well understood. The most common analysis of buckling of long slender devices is conducted using the Euler Buckling Equation. Under this model, there are only four parameters that can be changed to increase the critical buckling load P_{crit}. Under specific design constraints, there may be times that these parameters cannot be changed. In surgical equipment, the material properties and dimensions of members like a catheter or an endoscope are predefined and cannot be changed without changing the performance of the instrument. As the cross-sectional area of these members becomes smaller, the critical buckling load decreases as well. One approach to increasing the P_{crit} for a device is reducing the spacing between supported points. For a long member, additional supports can be added along the length to reduce the length between individual supports. For evenly spaced supports, the overall critical load for the entire member increases by a factor of $(n+1)^2$ where n is the number of supports. These supports must support a lateral load as the member tries to flex outward under the axial load.

For robot-assisted surgery, these lateral supports are part of a system commonly known as a anti-buckling guide or anti-buckling support system. For some robotic configurations, this support system must be able to fit within a specific dimensional constraint as well as compress through the insertion stroke. The compressibility of this system– the ratio of the stroke length over the full length– is directly tied to the usable length of the member. The lower the compressibility, the more of the member is unusable. This system must also be able to withstand buckling itself under the axial compressive insertion loads, along with the added lateral loading by the member as the member tries to flex out laterally. The system may also be aligned at an angle (as shown in Figure 1.1), adding an eccentric loading to the system due to gravitational forces.

A current anti-buckling guide system uses a pantograph (See Figure 1.2) to achieve the compressibility and the lateral support [3]. There are several versions of this system, but they are bulky and have a large number of parts, many of which are unique. The high part count, along with the intricate system could lead to high manufacturing and assembly costs and introduce difficulty in sterilization of the device. One method that is common in reducing part count, manufacturing and assembly costs, and increasing precision is replacing rigid links and joints with compliant mechanisms. Compliant mechanisms can also be designed for harsh environments [4], which could include those found in the autoclave cycle used in medical applications as a common way to sterilize medical equipment. Compliant mechanisms have been used in medical robotic systems design to reduce part count and size [5–7].

One collapsible compliant system that has been investigated for the protection of sensitive members is an origami-inspired bellows. These bellows have a high compressibility and fatigue life [8]. They can be designed for harsh environments as in space applications. The dimensions of the stroke and the inner and outer diameter of the bellows are free design parameters, but the choices made will have an effect on the functional properties of the bellows [9]. They also can be created out of a variety of materials.

Another common support system for long, thin, flexible members is to rigidly attach them to a stiffer object. There are many examples of such systems. For example, a widely used system is the support of electrical wiring. Long stretches of thin, flexible wiring is supported by power poles outside and through specified paths in the walls of buildings or the use of protective conduit . This method is used to guide wires to an intended location and maintain them in an area away from

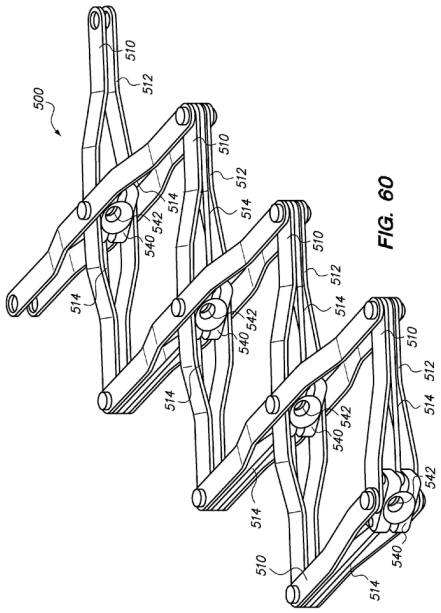

Figure 1.2: Image from patent application [3] for a pantograph support guide

possible damage. Although simplistic, this approach in its most basic level defines one of the most common ways to support and guide flexible members and these principles could be translated into other more complex mechanical systems.

In some of these members, the resistance to an axial load is so low, especially at longer lengths, that it could be modeled as a rope or cable. Typically in engineering, ropes and cables are assumed to be tensile members. However, a member in tension does not buckle, as buckling is a response to a compressive loading. Ropes and cables in tension also resist lateral displacement due to stress stiffening. If the tension is great enough, stress stiffening in cables provides a member that can be modeled as a rigid beam and could be used as an attachment point for supports that connect to the more flexible medical device.

In construction, for extremely long columns in structures, an exterior frame is often used to brace the load bearing member. One such system is the Buckling Restrained Braced Frame (BRBF) used primarily to protect against seismic activity [10]. This system supports the load through a

central steel column surrounded by a casing that through its flexural rigidity provides the central member with the lateral support that it needs to prevent buckling failure. This acts as if the number of support points was infinite, providing constant support along the entire length of the beam. This is unconventional in that it does not increase the critical load of the beam itself, but simply protects the buckling member from lateral displacement that leads to failure resulting in an increase in the load that the total system can support.

1.2 Research Objectives

The objective of this research is to further understand principles that can be applied in buckling mitigation to aid in the design of systems that support long, thin, flexible members for robot-assisted surgery. The development of design guidelines and metrics will be important in the understanding of the effectiveness of the systems developed through the applications of the principles investigated. The stiffness of the system to lateral perturbations is an important metric for these systems, and research into parameterizing this property is presented here. These principles and metrics are used to create several support systems to provide anti-buckling support to flexible members during operation. Consideration is made on part count and biocompatibility. These systems have been designed to be adapted to fit within the existing dimensional parameters of a surgical robot system.

The research has explored possible solutions, emphasizing compliant mechanisms due to the advantages explained earlier. The design space was narrowed down to the most promising concepts through analysis and testing. Decisions on each concept were be made based on the lateral and buckling support provided, compressibility, design feasibility, and manufacturing costs. Further testing and refinement of the chosen concepts was conducted. Working prototypes have been created and tested on an actual robotic system.

The subsequent chapters address the design process used in the selection of those concepts used in final designs. Three design concepts are presented: the Ori-Guide, the ZTR, and the Retractable Support Systems. Each chapter includes a discussion on important features, manufacture, and performance. This research also investigated the processing of Polyethylene Terephthalate (PET) films and the change in the physical properties as this material was important for the Ori-Guide System.

Chapter 2 will discuss the design process and the development of the concepts. Chapter 3 is a overview of the Ori-Guide concept, including the development of the pattern used and the testing of the final support system. Chapter 4 discusses the investigation of the heat setting process. Although this was used primarily for the Ori-Guide concept, this investigation was made general for PET film and origami patterns in general. Chapters 3 and 4 will be submitted for publication in a venue to be determined. Chapter 5 reviews the ZTR concept, following a similar flow as Chapter 3 moving from development to prototyping and testing. This chapter has been submitted for publication as a conference paper at The Conference on Reconfigurable Mechanisms and Robots. Chapter 6 presents the Wires in Tension and Orthogonal Beams concepts together as the first lead to the development of the latter. This chapter will be submitted as a conference paper at The International Design Engineering Technical Conference. Chapter 7 provides a conclusion and summary of the work presented herein.

CHAPTER 2. DESIGN PROCESS

2.1 Design Process

The project began with an exploration of the possible solutions. Observing the function of the current Anti-Buckling Guide (ABG) used by Intuitive Surgical Inc., solutions were investigated that provided similar motion and support to that given by the ABG. The search was then expanded to mechanisms that are collapsed during use, and mechanisms and systems used for support against buckling. These mechanisms and systems were sorted into four general categories and a design tree was created (Figure 2.1). Category one, Origami, was primarily inspired by previous work done at BYU. Category two, Minimalistic, focused on designs that occupied very little operating volume in the workspace. Category three, Compliant, looked into designs that that gained their motion from bending or stretching. Category four, Rigid Mechanisms, investigated designs similar to the ABG in that their motion was gained from a set of rigid links moving relative to one another.

2.2 Design Metrics

Using the project needs and design criteria, we created a set of metrics that could be used to evaluate our designs. This was helpful in the down selection process as well as in creating a testing protocol for the selected designs. The design metrics are listed in Table 2.1.

Table 2.1: Design Metrics

Primary Metrics	Secondary Metrics
Lateral Stiffness	Stiffness Ratio- Lateral/Axial Stiffness
Axial Stiffness	Distance between Support Points
Ratio of P_{crit} to Insertion Length	Part Count
Dimension of Support System	Sterilization
Cost	Manufacturability
Usability	Lifetime or Number of Uses
Ratio of Lateral Stiffness to Insertion Length	Aesthetics

2.3 Design Selection

In investigating each concept using the above metrics, down selection was made to a Kresling model, a modular origami zipper-tube model, a passively wound Buckling Restrained Braced Frame (BRBF) model, a wires in tension model, and a spring-inspired model. In further modeling and prototyping, it was soon decided that a multi-pattern Kresling would be the best option for the Kresling approach. The origami zipper-tube was discovered be difficult to actuate and manufacture. Investigation into various springs resulted in a determination that due to the particular constraints on system dimensions it would be difficult to create a spring that would function as desired while meeting the dimensional requirements. Mathematical modeling of the wires in tension concept discovered that it would require too much to force to keep the system in tension sufficient to add the desired lateral stiffness for the robot system used at Intuitive Surgical. However, work in this area would act as a springboard for the orthogonal beams idea. Due to their similarities, these two designs were analyzed together as the Retractable Support Systems.

This down-selection led to three major concepts: the multi-pattern Kresling (the Ori-Guide), the BRBF concept (the ZTR), and the Retractable Support Systems. Each design concept will be discussed in greater detail in the following sections. Each chapter also includes a discussion on how the concepts were tested.

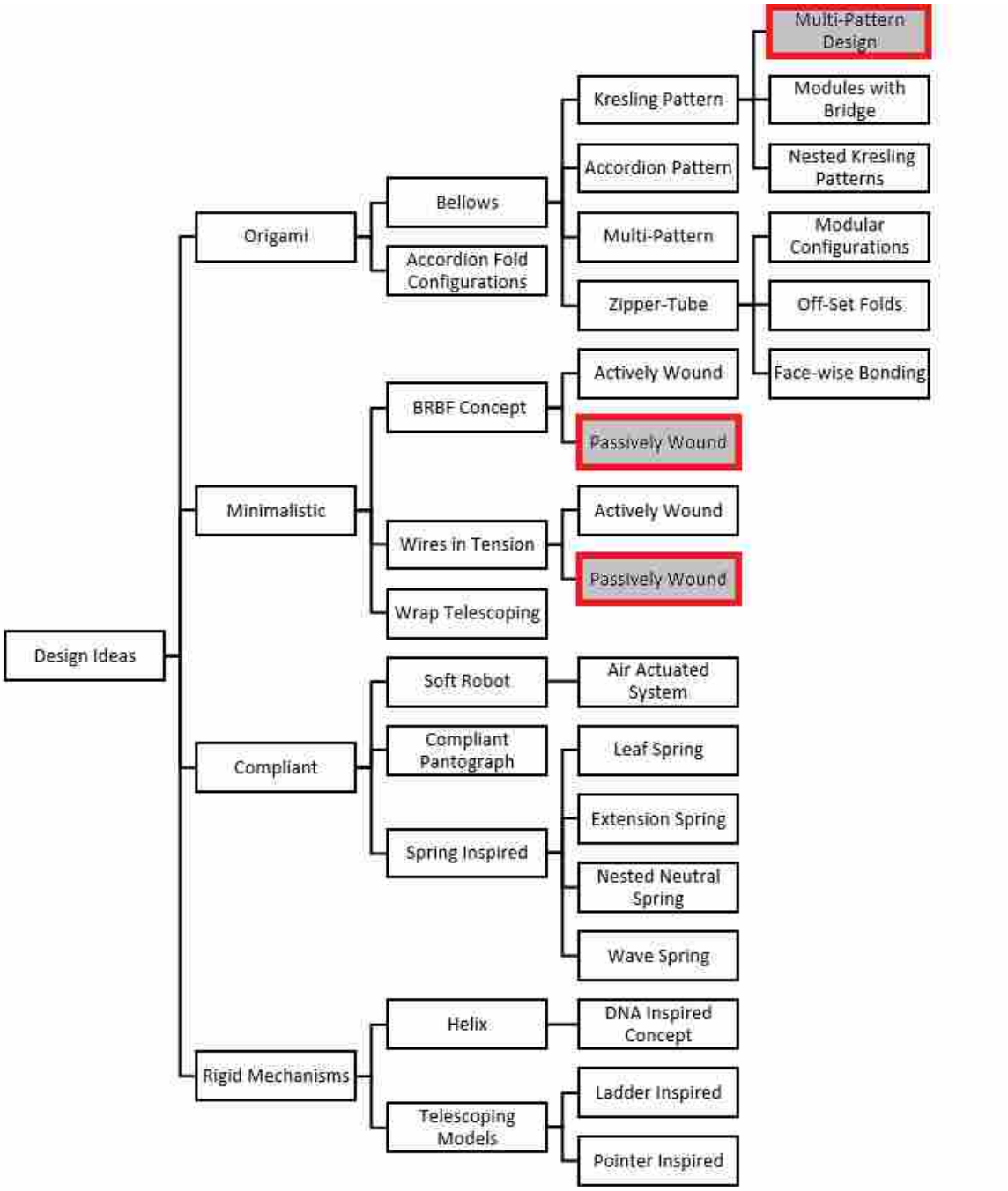

Figure 2.1: Design Tree of all the fundamental ideas considered for use in buckling mitigation. Design ideas that were pursued further are highlighted.

CHAPTER 3. ORI-GUIDE

3.1 Ori-Guide

One branch of compliant mechanisms is origami inspired design. Origami, the art of paper folding, can create intricate structures, mechanisms, and sculptures. Analysis of origami and its motion has already inspired other medical devices [5–7]. In [5] a robotic gripper was reduced to a single part through a study and modification of an origami pattern. Study of compliant mechanisms, especially in the area of origami, inspired the design of a novel anti-buckling support system that reduces the part count while adding other enabling features to the support system.

3.2 Origami-Based Anti-Buckling Support System

An origami-based system, the Ori-Guide, has been crafted using an origami tube-like structure made from a single sheet of flexible material. The proposed origami pattern integrates supporting and actuating layers that enables the anti-buckling system to expand and compress and have discrete support points, analogous to the pantograph, while being manufactured from a single flexible sheet. The support layers are designed to have a smaller inner diameter which remains constant throughout the stroke. This diameter can be designed to fit the instrument size. These supports can be evenly spaced through the pattern to provide staged support of the instrument. The pattern can also be designed such that the supports are spaced in a specified pattern for instruments that require more support in one area than another. Rigid mounts connect the origami mechanisms to the robot, resulting in a support system of only three parts.

3.2.1 Pattern Overview

The origami pattern used in the Ori-Guide is a modified version of a triangulated cylinder pattern shown in in Figure 3.1a, also known as the Kresling pattern [11]. With this pattern, the

outer diameter D_o, folded inner diameter D_i, and story heights can be adjusted. The pattern and these parameters have previously been determined as described in [11–16].

The pattern is defined by five basic parameters: a, b, and c form a tessellated triangle, n is the number of sides or number of times the triangle tessellation is repeated per story, and s represents the number of stories of the bellows (See Figure 3.1a). These parameters are a function of D_o and D_i, and n.

$$a = D_o \sin(\phi) \tag{3.1}$$

$$b = D_o sin\left(cos^{-1}\left(\frac{D_i}{D_o}\right) - \phi\right) \tag{3.2}$$

$$c = D_o \sin\left(\phi + sin^{-1}\left(\frac{b}{D_o}\right)\right) \tag{3.3}$$

$$\phi = \frac{\pi}{n} \tag{3.4}$$

These parameters aide in design as the inner diameter will play the primary roll in support of the instrument and the outer diameter is usually constrained by robot geometry. Other parameters that define the motion and behavior are: h, the deployed height per story, δ the deployment angle of a story as illustrated in Figure 3.1b, and the Stability Transition Ratio (STR) discussed in the next section. δ varies from 0 rad (fully compressed) to the maximum deployment of the specific pattern configuration ($< \frac{\pi}{2}$) determined by the strain in the pattern. These parameters enable the development of this new pattern and application.

$$h = b \sin(\delta) \tag{3.5}$$

Bistability Analysis

During actuation, this origami pattern will exhibit either monostable or bistable behavior. This is due to the fact that the pattern is not rigid-foldable, meaning that the panels, not just the

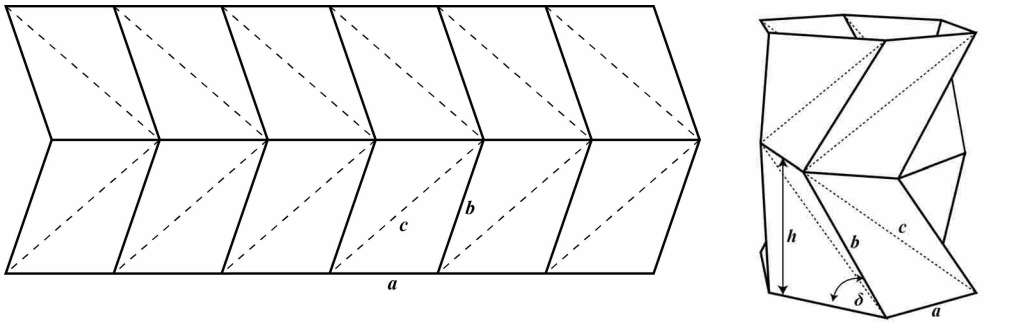

(a) $n = 6$ $s = 2$ pattern with defining parameters (b) Pattern in Fig. 3.1a folded into tube

Figure 3.1: Example of the triangulated cylinder pattern from which the Ori-Guide was developed

creases, must strain to actuate in this configuration. The bistable or monostable behavior is a function of n and the ratio between D_i and D_o. Previous work has been done to predict the bistable behavior of each story of the pattern by assuming the lengths of a and b are fixed and the only flexing comes in the length of c, neglecting the strain in the panels [15]. By this assumption, the dimensionless strain energy, w, through the actuation can be represented by

$$w = \frac{1}{2}\left(\frac{c(\delta) - c_o}{c_o}\right)^2 \tag{3.6}$$

where c_o is the initial length of c and $c(\delta)$ is the length of c as a function of the deployment angle δ

$$c(\delta) = \sqrt{\left(D_o sin\left(\phi + sin^{-1}\left(\frac{bcos(\delta)}{D_o}\right)\right)\right)^2 + (bsin(\delta))^2} \tag{3.7}$$

Note that as δ goes to zero, Eq. 3.7 reduces to the equation for c found in Eq. 3.3.

Graphing w over δ from 0 to 2 rad will give a strain energy curve for a given geometry. By changing D_i for a given D_o, a group of curves are found as shown in Figure 3.2. The curves with a second energy well (represented by the dashed lines in Figure 3.2, the higher humps correspond to smaller values for D_i) represent geometries with a bistable nature. The curve closest to developing a second energy well will result in the largest height per story. The ratio of D_i/D_o corresponding to that curve is called the Stability Transition Ratio (STR). This results in the smallest monostable D_i for a given D_o. This is desirable because the reduced number of folds increase the lateral stiffness. It was also discovered that due to the assumptions made in the strain energy analysis, along with

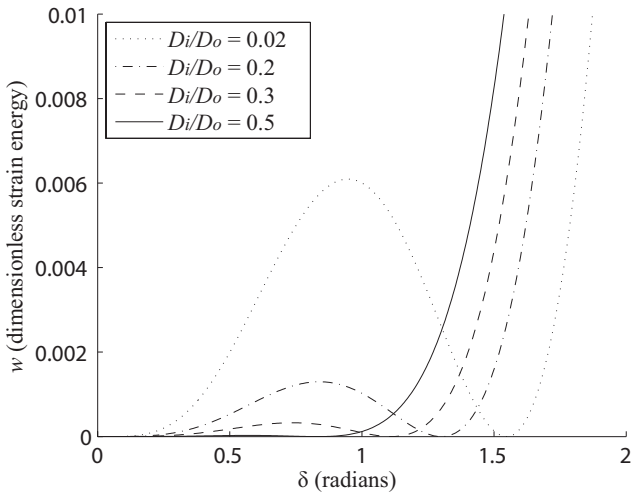

Figure 3.2: Strain energy curves for 4 different D_i for a fixed D_o. The solid line shows a monostable geometry where the second energy wells in the dotted lines show a bistable geometry. The higher the hump, the smaller the corresponding D_i and the more bistable the response during actuation.

the flexibility in the material, the inner diameter could be decreased just under that predicted by the STR while still remaining monostable.

Multi-Pattern Design

The inner diameter of the pattern will increase as the model deploys, which will not provide support to an instrument running through the pattern. A solution to this problem was developed by combining multiple variations of the pattern into a single model. This way the entire model can remain monolithic while incorporating areas with fixed inner diameters for support of an instrument running through the center of the bellows. The multi-pattern design is a made by repeating a number of stories with different behaviors. Monostable layers provide for the actuation of the model. These layers rotate during actuation. Every other monostable layer can be mirrored, which can cancel the overall rotation of the model during actuation.

Bistable stories, with a stable position in a closed (compressed) and an open (extended) position, can be used to support an internal instrument. This bistable story can remain in the closed position, which means no actuation would occur in that story and the inner diameter would not change. An adhesive may be used to adhere these bistable stories in the closed state. Once col-

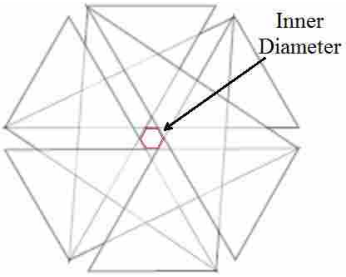

Figure 3.3: Section view of the support layer in the folded state. The inner diameter is designed to match the internal member diameter.

lapsed, these closed layers have a section view like that shown in Figure 3.3. These stories provide the support points for the instrument. Figure 3.4 shows the support layers in a prototype with a 4.5mm diameter catheter. This provides the added advantage of being easily designed to any instrument dimension, as the collapsed inner diameter of the bistable layer can be chosen using the equations in the previous section.

A computer program has been created using the equations that define the pattern and the strain energy to help with quick modeling of the pattern. This model receives inputs of D_o, D_i, and n and will return a, b, and c to use in creating the pattern as well as the propensity toward bistable behavior. Using this program, a full pattern can be designed while predicting the behavior of each story.

3.2.2 Tension

During the operation, the support system will actuate from a fully extended point to a partially to fully compressed point. One advantage of the pantograph system is that there is no point to which the system naturally returns. The Ori-Guide acts similar to a spring with a set natural length to which it wants to return. As buckling is a compressive force phenomena, compression springs have the possibility of failure due to buckling. Tension springs will never fail in buckling because as they are actuated, they want to return to their initial, fully compressed state, thus putting the spring in tension throughout the stroke. Using this idea, the natural length of the Ori-Guide can be designed to be in a fully compressed state, similar to that of a tension spring. With a material such as some polymers the natural length of the model can be changed using a heat set. Therefore

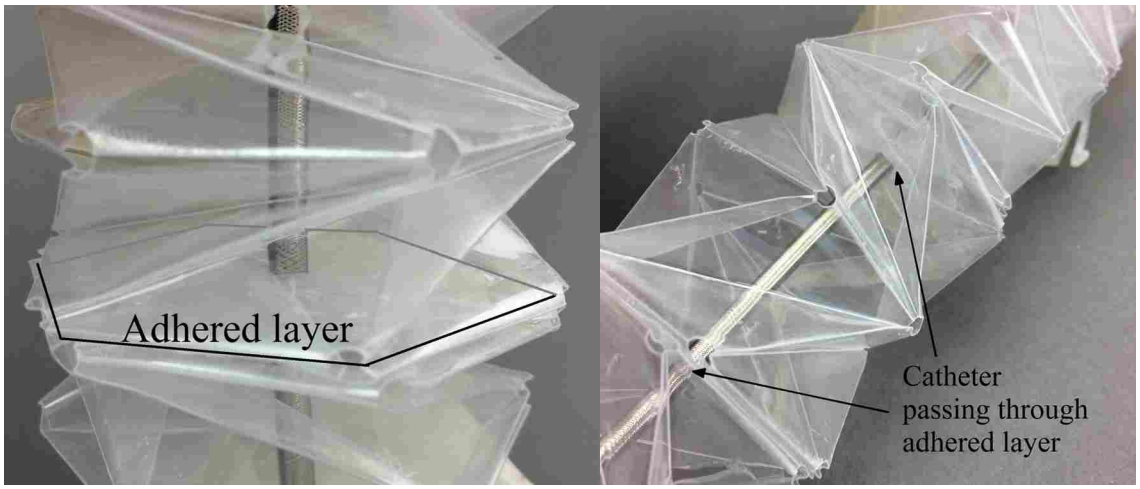

(a) Demonstration of two support layers with the actuation layers in an extended state

(b) Close up of a single adhered support layer with catheter passing through the center

Figure 3.4: Image showing the catheter going through the support layers

the system will always be in tension during actuation, removing any tendency towards buckling itself. The higher the tension, the more the robot will be required to pull to retract but will make the system more laterally stiff.

3.2.3 Heat Setting

A thermo-plastic polymer can be deflected to a desired shape, which places the part under stress. Then, adding the right amount of heat to the polymer causes the weak bonds between the polymer chains to break and the chains become more mobile, which allows the molecules to flow. The polymer chains can re-align and lower the amount of stress in the part. The cooling rate of the plastic can be controlled, which helps the polymer chains re-form in this new, low-stress state. This can cause the deflected shape of the part to be the new natural state of the polymer. Information on the heat setting process used in the physical prototypes tested can be found in Chapter 4.

3.3 Physical Validation

To create a full anti-buckling support system, bistable stories were combined with monostable stories in an alternating order. The exact parameters used in the prototype tested can be found in Table 3.1. The testing prototype has 18 monostable layers with 8 bistable layers in-between each

monostable layer pair. The bistable layers, when collapsed, create a inner diameter of 4 mm. The total device length when extended was just over 500 mm and compressed to just under 50 mm. It should be noted that the number and height of stories can be manipulated to tailor the performance and total extended length. An even number of monostable layers was kept in order to cancel individual layer rotation, so the overall rotation of the device remained at zero during operation.

The maximum strain occurs at the vertices; therefore failure would initiate at those points. To avoid failure holes can be laser cut into the sheet at the location of all the vertices of the folds. By removing the vertices, the axial force to actuate can be reduced, as well as the strain in the panel. By reducing the strain, the noise during actuation can also be reduced.

Once the model was heat set, tension was induced in the system to mitigate buckling, but near full insertion where the system becomes closest to its natural length, the tension drops to zero. Tabs can be included to extend over the compressed tube to help support the system laterally near full compression. To increase the performance of the support system near full insertion lengths, 45 mm length tabs were added to the mounts to which the bellows pattern attaches (See Fig. 3.5). The mount tabs, on both the proximal and distal mount, can be oriented so they interlock when the device has reached full compression. A locking feature was added to the tabs such that the device could be locked in the fully compressed state for ease of transport and storage.

A full concept drawing of the prototype shown side by side with the testing prototype is shown in Figures 3.6 and 3.7.

3.3.1 Testing

Comparative testing was done to assess the effectiveness of the Ori-Guide to an existing pantograph-based anti-buckling support system. This was done in two tests, a static and a dynamic loading condition. The static test was performed by fixing the support systems at a given length.

Table 3.1: Parameters for Physical Model

	a (mm)	b (mm)	c (mm)	n	Material	Thickness (mm)
Actuation Layers	27.5	36.01	51.97	6	PET	0.127
Support Layers	27.5	45.51	55.83	6	PET	0.127
Adhesive Film					PET/Acrylic Adhesive	0.0508

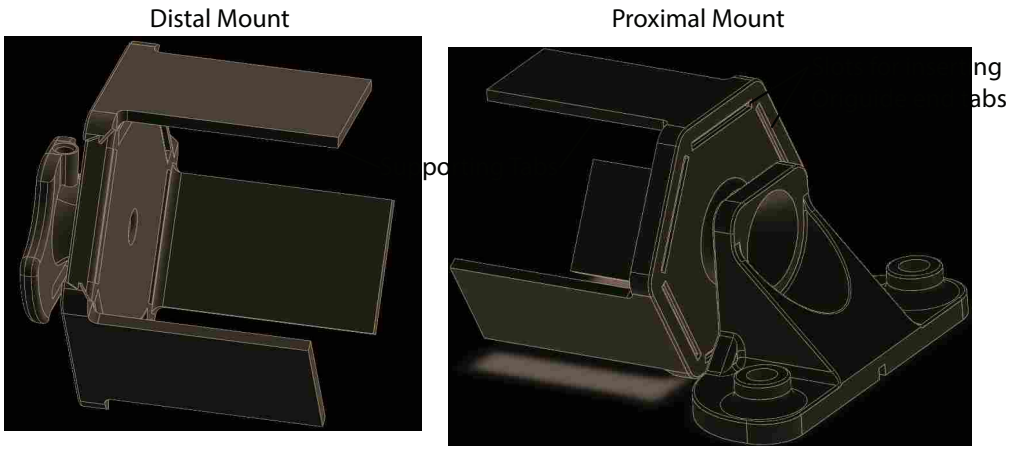

Figure 3.5: CAD models of Ori-Guide distal and proximal mount. Mounts were designed to adapt to a robotic system already in use.

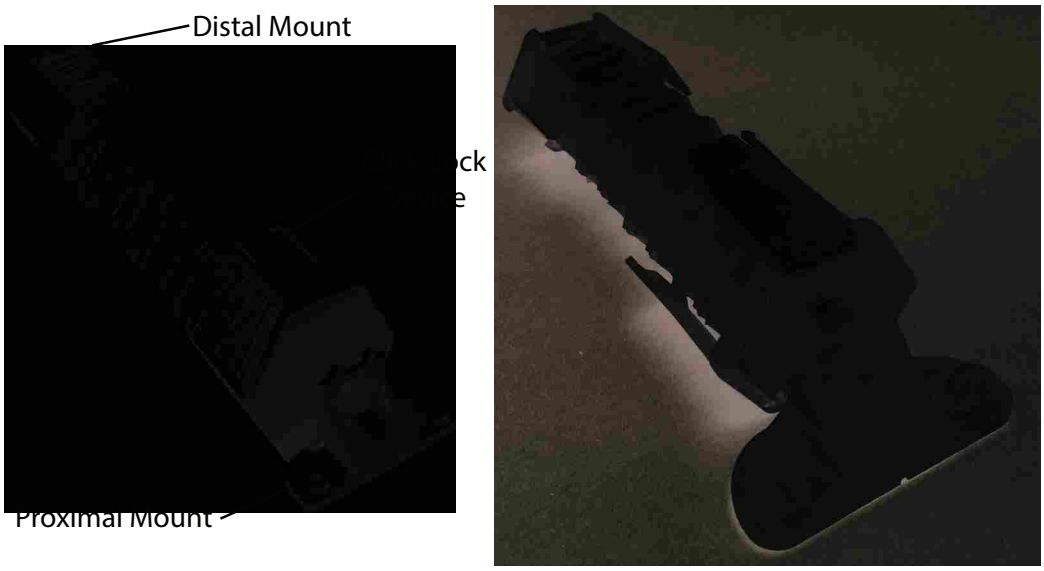

Figure 3.6: Origami Based Anti-Buckling Support System concept drawing and prototype photo of the model in the extended state. A locking mechanism was added to the tab to lock the device in the compressed state for ease of storage and transport.

A 4.5mm diameter biopsy catheter used in robotic surgery was inserted into the support system. The catheter was loaded with an axial compressive load until failure. Failure was determined if the catheter buckled under the loading or the catheter began to sustain damage due to crushing. The force to failure for the given length was recorded. This was recorded along a set of lengths

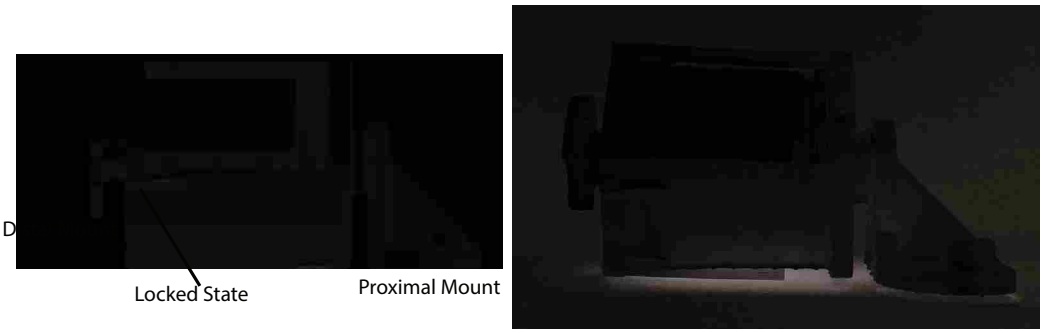

Figure 3.7: Origami Based Anti-Buckling Support System concept drawing and prototype photo in fully compressed and locked state. This is how the product could appear when removed from packaging and attached to the robot. The guide would then be unlocked and extended.

from 0 m to 0.4 m in increments of .05 m. Lengths were measured relative to the fully compressed position. This test evaluated the change in the critical buckling load, P_{crit}, of the catheter. The results of the static test can be found in Figure 3.8. No results were given for lengths under 0.2 m as the catheter would not buckle in either support system at these lengths but failed in another way. For the unsupported catheter, a value above 0.15 m could not be determined as it began to buckle under its own weight.

The dynamic test was performed on a surgical robot system by starting the robot arm at a given length. The catheter was fixed at both mounts and the robot arm was advanced from the starting length until the catheter failed or the support system buckled. The force applied was measured with the peak force before failure recorded as the dynamic critical load for the given starting length. This was compared to the existing anti-buckling support as in the static test. The set of starting lengths was similar to the set used in the static test. Each support system was driven through the entire stroke without the catheter to measure the friction and actuation forces needed to actuate the robot arm and support system. These values were subtracted from the forces measured in the dynamic test to show the amount of force transferred to device. The dynamic critical loads for a given starting position for both support systems are shown in Figure 3.9. No results were given for lengths under 0.1 m as the catheter would not buckle in either support system at these lengths but failed in another way.

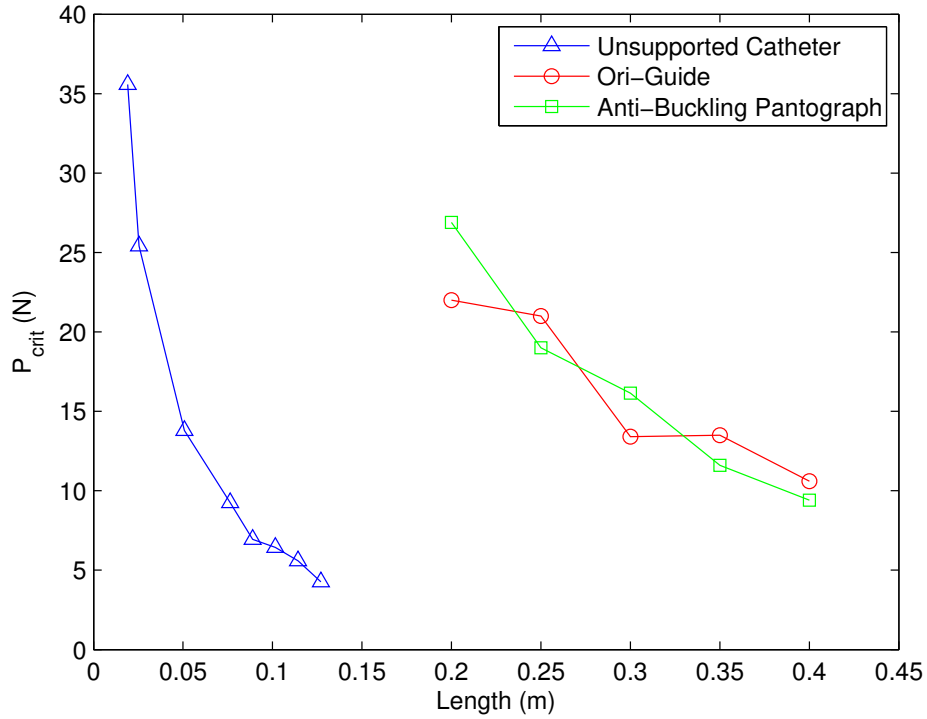

Figure 3.8: Static test results evaluating the critical buckling load of a catheter. The catheter would begin to crush for lengths below 0.2 m while in the support systems. Values above 0.15 could not be determined for the unsupported catheter as it would buckle under its own weight.

3.4 Discussion

3.4.1 Test Results

In both the static and dynamic test cases, the Ori-Guide support system performs very similar to a the pantograph system. Both systems show a high superiority to the unsupported catheter and provide an increased resistance to buckling loads. In both tests, the systems supported the catheter in such a way that at lower lengths no buckling occurred. Both systems displayed this behavior at about the same length. The tension added through the heat set allowed the Ori-Guide to continue to perform equivalent to the rigid system, even at large lengths.

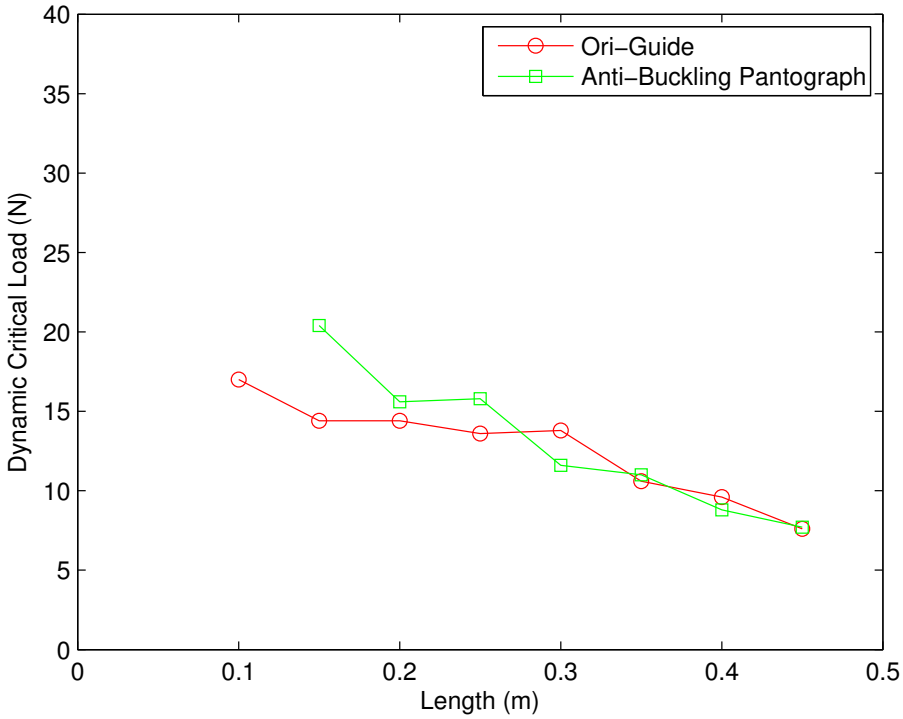

Figure 3.9: Dynamic test results evaluating the dynamic critical load of a catheter. The catheter would begin to crush for lengths below 0.1 m while in the support systems.

3.4.2 Enabling Features

The origami-based system has several features that could enable further developments and improvements to the robot surgical systems and operations. Primary among these is the ease with which this system can be changed to accommodate other sizes of internal members. This pattern is mathematically described and for a different internal instrument size, a different D_i can be selected for the bistable support layer, allowing the pattern to be quickly and easily changed. It can also be tailored to any D_o as long as it remains feasible to manufacture. Because the design is origami-based, the number of parts is not a function of the desired stroke length as it would be in a rigid system.

Due to the origami bellows style design of the Ori-Guide system, the device remains largely enclosed by the support system. This provides additional protection against airborne pathogens that could contaminate the device and also reduce the risk of pathogens from the patient carried on the

device from being released into the surgical space. Pantograph-based devices have large open areas where the device is vulnerable to contamination.

3.4.3 Other Applications

This origami-based anti-buckling system can also find application in other areas. This system has application in tube structures where a variable orifice is needed. This can include pumps or throttle systems, all of which can be made from a single material. The design can also be made to completely close the tube with a bistable layer with an inner diameter of zero, which can create built-in caps or valves in the tube. The model could allow flow in the open stable position and actuate to the closed stable position, closing off flow.

3.5 Conclusion

The Ori-Guide support system has proven to be equivalent in anti-buckling performance to a rigid counterpart. The origami based design drastically reduced the part count compared to rigid systems evaluated and holds a constant part count for systems of different lengths. The novel pattern developed is highly customizable and can therefore be easily changed to fit varying devices. The design of the Ori-Guide protects the device from external contamination over a rigid system. The features of the Ori-Guide system could also find application in other areas.

CHAPTER 4. HEAT-SETTING

4.1 Introduction

Origami is the ancient art of paper folding. In the recent years, origami has been investigated for use in engineering applications. It has many advantages that are not readily available in traditional engineering mechanisms and design techniques, including being monolithic, being highly compressible and compact, and achieving all motion through compliance. Many of the patterns are easily tessellated and some patterns create metamaterial behavior, causing the mechanisms to exhibit interesting motion uncommon in traditional materials or mechanisms [17]. There has been a great deal of study on the many uses of origami and the parameters that define the characteristics of the various fold patterns [18, 19].

Another benefit to origami inspired design is that there are many materials that are compatible for use in origami design. Although there have been techniques developed to expand origami-based design beyond sheet materials, for a material to be useful in traditional origami patterns it must be a sheet or film with negligible thickness and be stiff enough to be able to hold a crease. For example, Butler et al. investigated using Mylar, Tyvek, Kapton, UHMWPE, and ETFE for their application [14]. This study will investigate the use of Polyethylene Terephthalate (PET), a common polymer often found in thin sheets and in applications such as consumer liquid containers. Due to the availability of PET and favorable characteristics of the PET sheets for origami folding, it has been considered for use in origami design.

The usefulness of a material for origami applications is the ability of the material to hold a crease. This is defined by the ability of a sheet to be folded upon itself and, after pressure is applied and released on the crease, stay in the new folded configuration. The pattern can then be actuated away from the folded configuration and after actuation, still retain a bias toward the folded configuration. Some materials, like many consumer fabrics, do not hold a crease or exhibit only a small bias towards the folded configuration when a crease is formed. Other sheet materials, like

metals, fold and hold a crease but they are limited to the one folded state as strain hardening at the crease causes the material to not actuate at the crease. This may be desirable for some static situations, but for action origami or origami mechanisms, some degree of motion is required from the pattern. For origami applications in engineering, the properties of the crease are important design factors. Polymers often have larger elastic regions then metals, allowing them to undergo larger deformations and actuation at creases before yielding. Due to the stiffness of PET, PET films are a good candidate for origami applications as they can hold the crease with spring-back toward the folded state. This work investigates the effects of processing methods on the force response of the creases in the film material.

PET is a semi-crystalline thermoplastic polymer. This means that a PET sample is a combination of amorphous pockets and crystalline lamellae [20]. The degree of crystallinity has a large effect on the physical properties [21]. PET also has a relatively high glass transition temperature (T_g) and a slow crystallization rate. These characteristics lead to highly different physical properties based on the processing of the polymer. The stresses placed on the polymer and the heating process are two of the largest contributors to the crystallinity and orientation of the molecules. Work has been done to investigate the effect of processing and crystallinity and crystal growth on PET films and fibers [20–24].

Amorphous PET has a cold-crystallization temperature of $T_c \approx 135^o$C [24]. Cold-Crystallization is when the polymer is heated above glass transition ($T_g \approx 75^o$C for PET) and the molecules can move sufficiently to start to organize into crystalline structures. These will eventually melt as it approaches the melting temperature ($T_m \approx 250^o$C). Flores et al. [20] studied the various levels of crystallinity of samples annealed at temperatures from $100 - 190^o$C for 9 hours to induce cold-crystallization. Samples annealed at lower temperatures started with a lower crystallinity. When heated again at 2^oC/min, all samples reduced in their level of crystallinity initially, but those annealed at a lower temperature (less than 160^oC) then increased in crystallinity when passing the annealed temperature until reaching T_m. Similar but not as prominent trends were seen at heating rate of 40^oC/min. They observed that the higher heating rate limited the reorganization of the internal polymer structure.

Karagiannidis et al. [22] discovered that PET films can increase in crystallinity under the cold-crystallization temperatures. They annealed their samples at 115^oC for 0-30 min and noticed

an increase of crystallinity of up to 30%. Abou-Kandil and Windle [23]focused on the formation of the microstructure of amorphous PET samples as they were drawn and then annealed. They found that when a sample is stressed in a direction, a mesophase liquid crystalline phase is formed prior to full crystallization. This phase is of a smectic-A structure. They also found that the chains of the polymer arranged themselves in the direction of the draw.

Cho et al. [21] showed that for a short heat treatment in a free-to-relax condition, PET fibers would lower the yield stress while maintaining a high elastic modulus. This was due to the formation of micro-crystals in the heated areas. The heat treatment was for just over 1 s at around 190^{o}C. Similar results were found with heating as-spun fibers with a CO_2 laser [25].

The strain rate also plays a role in the crystallinity of the final PET produce. This is due to strain-induced crystallization. Martins et al. [24] observed that strain hardening occurs in two phases: 1) a smooth increase in stress with rapid increases in crystallinity up to 15% crystallinity and 2) a sharp increase in stress with little change in crystalline structure. For very high strain rates, the crystallization did not occur until after the motion and was greater than when strained at lower rates or at high temperatures. They concluded that slower speeds at high strains helps improve the organization of the crystals. This also helps with thickness uniformity. However, for higher crystallinity and higher orientation at the end of the process, use faster speeds at higher strains.

Applying this knowledge, this study investigates several processing methods and their effect on the force response of folded PET film samples. As the material properties change as a function of processing, the tailorability of the force response is investigated. Tailorability of the response is important as the applications for origami engineering vary.

4.2 Methodology

4.2.1 Sample Manufacturing

Clear PET film from McMaster-Carr were obtained for use as samples. The samples were 0.127 ± 0.0127 mm. Using a CO_2 laser, equally spaced fold lines were etched into film strips. This was done at 3% of the laser power to score the film without cutting it. The laser was used to ensure the accuracy and repeatability of the fold pattern. To ensure that the laser scoring did not adversely affect the samples, strips of scored and unscored PET films were tested in a tensile test.

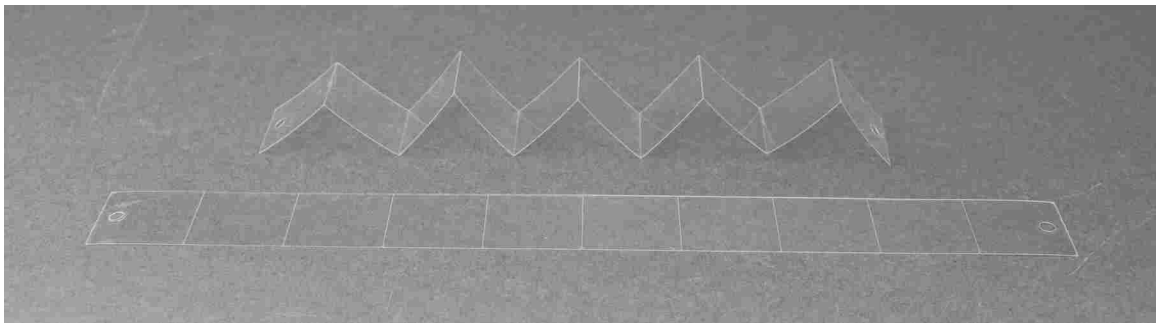

Figure 4.1: A scored sample before folding (bottom) and a scored and folded sample (top). Holes used to attach to the tensile tester can be seen in the first and last panel of the sample strips.

The laser had little effect on the elastic modulus of the plastic, which corresponds with the findings in [21, 25] for PET fibers. It was determined that in the working range of stresses, the use of laser scoring would not have an adverse effect on the final performance of the origami models.

Strips of PET 254 mm by 25.4 mm were cut with lines scored every 25.4 mm along the length creating 9 folds and 10 panels. Holes were cut in the first and last panel for attachment to the tensile tester. A simple z fold was folded into each test sample. Folded and unfolded scored sample strips are shown in Figure 4.1. Tensile tests were performed on a set of randomly selected test samples to ensure that there was not a significant difference in the samples.

4.2.2 Processing

Samples were labeled, folded, and pressed into a fully compressed state between two thin aluminum plates. Each pattern was processed in batches of 10 samples using a combination of the processing variables described in Table 4.1, resulting in 60 distinct batches. Preliminary testing on a wide range of times and temperatures between T_g and T_m, as well as cooling methods, was conducted to narrow the range of the variables used to those in Table 4.1. The preliminary testing was not intended to completely search the space but to narrow the testing range to a more manageable set of testing processes. Preliminary testing showed low force responses and high relaxation when the samples were cooled rapidly through T_g. This could be attributed to the high cooling rate not allowing for the reorganization of the internal polymer structure as was similarly seen during heating [20]. Two rates of cooling the samples were used. The first, an annealing referred to hereon as

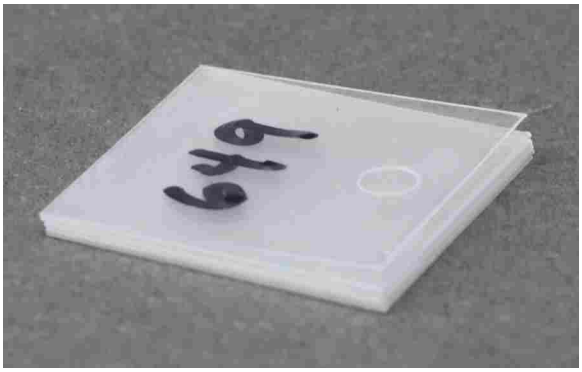

Figure 4.2: Sample 649 given as an example of how the sample strips appeared after processed in the folded position

"Slow Cooling", was performed as the samples were allowed to cool in the oven back to ambient temperature T_a. In the second, referred to as "Drop Cooling", the air temperature in the oven was quickly lowered to 90^{o}C (approximately 15^{o}C/min) and then the samples were slowly cooled from 90^{o}C to T_a (approximately 0.5^{o}C/min). This cooling method slows cold-crystallization similar to quenching but allows for some reorganization by slowly passing through T_g.

After processing, the samples were removed from the plates and a thin knife was run between the panels to ensure there was no adhesion between the panels. Figure 4.2 shows the sample labeled 649 as an example of how the sample strips appeared after processing.

Table 4.1: Variables used in processing methods for the sets of test samples

Heating Times (min)	Temperatures (^{o}C)	Cooling Rates
60	120	Drop
75	130	Slow
90	140	
105	150	
120	160	
	170	
	180	
	190	

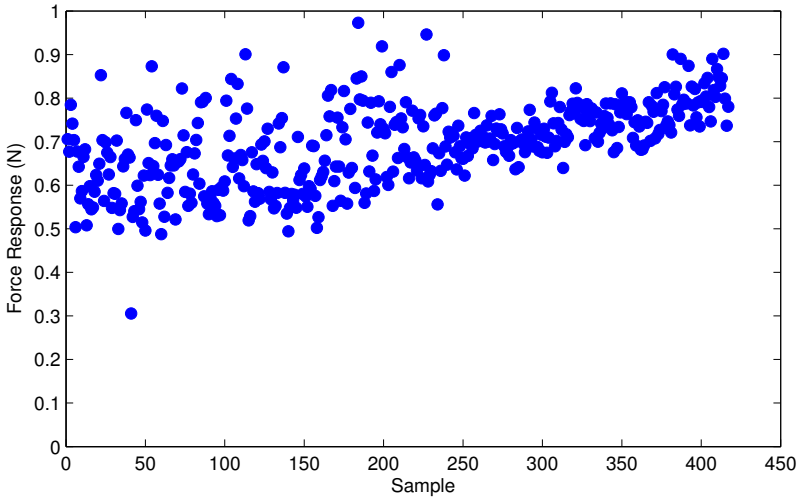

Figure 4.3: Force response of all samples

4.3 Evaluation and Results

4.3.1 Testing

Each sample set was tested under two different loading conditions. First, 8 samples from a batch were individually pulled in a tensile test to 165 mm and then returned to their initial length. The force-deflection relationship was observed for both the extension and return. The maximum force response was recorded and an average for all 8 samples was recorded. The standard deviation of each sample batch was also recorded. The force response of all the samples is shown in Figure 4.3.

The second loading condition was designed to determine the effect of stress relaxation. 2 samples were individually pulled to 165 mm and held for 20 seconds. The force-time relationship was observed. The initial maximum force exerted by the sample and the final force exerted were noted. The difference was recorded as the “Force Drop” and the percent decrease of the initial maximum force was evaluated and recorded. The Force Drop of each sample is shown in Figure 4.4.

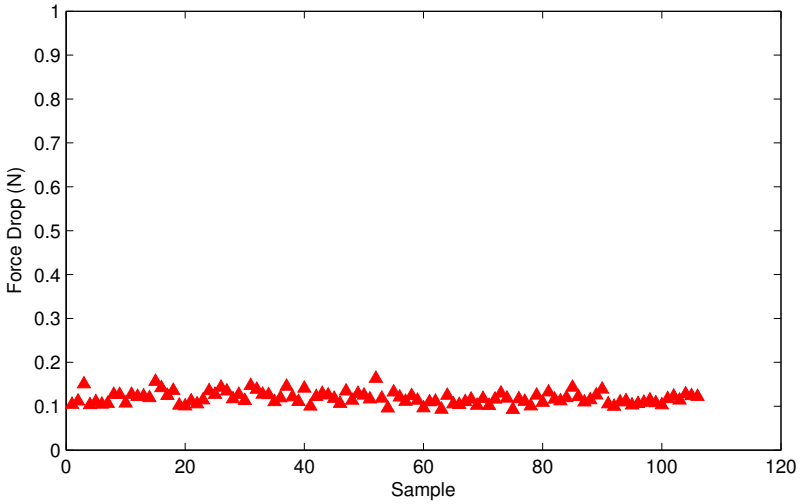

Figure 4.4: Force Drop of all samples

4.3.2 Observational Data

As crystallinity increases in PET, the haze of the polymer increases [26]. Before heat treatment, the sample strips were transparent, corresponding to a low crystallinity. After treatment, the samples became hazy. Samples treated at higher temperatures showed a greater haze than those processed at lower temperatures. In the range of times for a given temperature, those that were heated for longer times appeared slightly more hazy than those at lower times. No observable difference could be made between cooling rates. Figure 4.5 shows samples 503 and 708. Sample 708 was heated for 60 min at 150 C with a drop cooling. Sample 503 was heated at 170 C for the same time and cooling as sample 708. A significant increase in the haziness corresponding to the increased processing temperature.

As the temperatures increased above 170^{o}C, adhesion became increasingly pervasive in the panels until melting the panels together. Slight adhesion was observed at the cut edge (where the laser cut the sample from the main polymer sheet) at all temperatures, but at temperatures above 170^{o}C, significant adhesion in the panels themselves began to be observed.

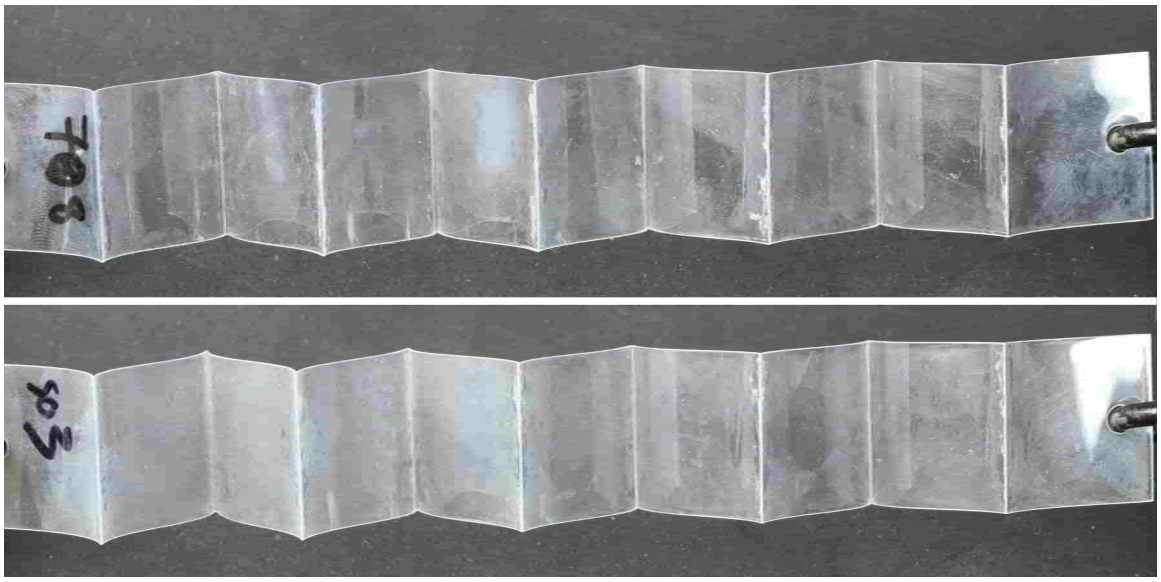

Figure 4.5: Samples 503 (bottom) and 708 (top). Both were treated with the same time and cooling, but 503 was processed at 170 C and 708 was processed at 150 C. A significant increase in the hazy can be seen corresponding to the increased processing temperature.

4.3.3 Discussion

There was only a small deviation in the force responses between variations in heating time in the range of 60 to 120 minutes and the cooling times. However, the processing temperature demonstrated a large effect on the force response. Grouping all the samples tested for force response by temperature with the standard deviation of the group is shown in Figure 4.6. A steady increase in force response and decrease in variability of the force response can be seen with an increase in temperature.

The lowest force drop represents the model with the least stress relaxation. Little deviation was seen between all the processing variables and the Force Drop as seen in Figure 4.4. Grouping the Force Drop samples by temperature as in Figure 4.6 yields Figure 4.7.

As crystallinity increases in PET, the haze of the polymer increases [26]. Flores et al. also found that for PET films starting with a low crystallinity, when reheated above T_c, there is an increase in crystallinity corresponding to the increase in temperature. Therefore the samples processed at higher temperatures obtained a higher degree of crystallinity. This increase in processing temperature also correlates with the increase in force response. Less variability in the sample force

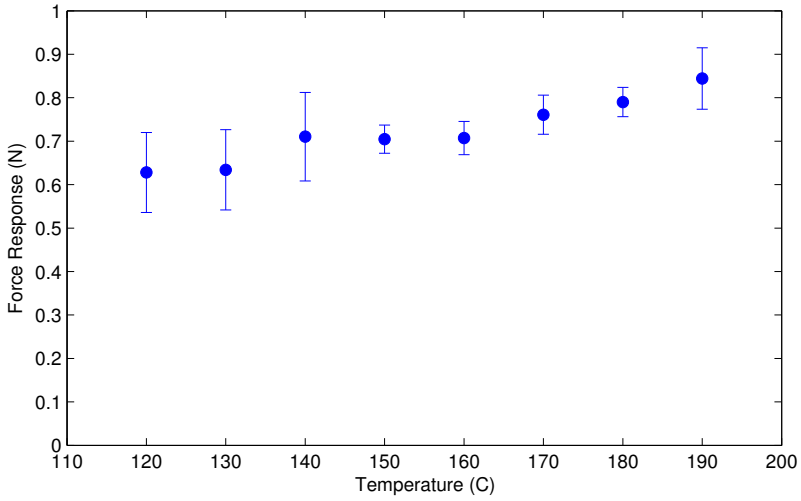

Figure 4.6: Force response of samples grouped by processing temperature. Bars represent standard deviation from the mean value.

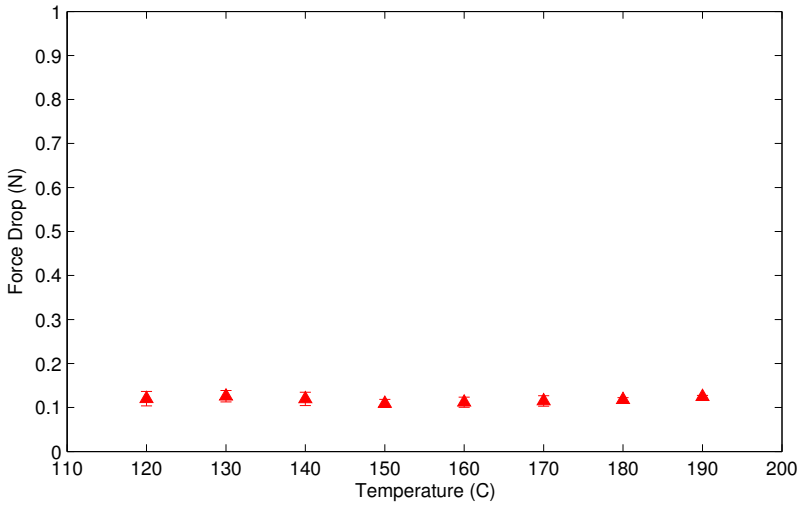

Figure 4.7: Force Drop of samples grouped by processing temperature. Bars represent standard deviation from the mean value.

response was also seen in temperatures above T_c than near to or below T_c. Crystallization in the folded state appears to have a large influence on the crease properties of the processed PET films.

Due to the adhesion in the panels at higher temperatures, which would be detrimental to most origami applications, temperatures from 150-170^{o}C are good candidates for treatment of origami models.

4.4 Physical Validation

A processing method of 170^{o}C for 60 minutes with drop cooling was applied to several different patterns to show application in various origami patterns. This method was chosen for physical validation because of the high force response and below average relaxation. The patterns were processed in a desired position and the motion and bias of the pattern was observed.

The first is a triangulated cylinder origami pattern colloquially known as the Kresling pattern. Recent work at BYU has investigated the use of this pattern for several applications in space technology [14, 16]. In these studies, Butler et al. focused on using the Kresling pattern for shielding for sensitive mechanisms on spacecraft. Many previous studies have investigated the characteristics of this pattern [11, 15, 27].

The Kresling pattern is defined by a repeated triangular tessellation wrapped into a tube. This particular pattern is not rigid-foldable, meaning that some strain is introduced into the creases and panels during actuation. This behavior increases the tendency of the model to return to the initial position or "natural length" similar to a spring. This can be advantageous if the design application requires axial stiffness. Stress relaxation also becomes important if the pattern is designed to be used in an application where it is held away from the natural length for long periods of time. Therefore, the natural length and the amount of axial stiffness and the amount of stress relaxation are important factors for using this pattern in design.

Implementing the process method discussed, it was shown that the natural length of the pattern could be changed from the extended position inherent in the manufacturing method to a fully-compressed state. One of the test models before heat treating is shown in Figure 4.8a. The same model after treatment is shown in 4.8b. The models in Figure 4.8 use blue tinted PET 0.1778 mm film to show that the heat set applies to a variety of films. An example of the pattern in clear 0.127 mm film can be seen in Chapter 3 in the Ori-Guide support system.

To prove the application of self-deploying patterns, the Miura-Ori tessellation was analyzed. This pattern was chosen as it is a basic tessellation, variations of the pattern have many

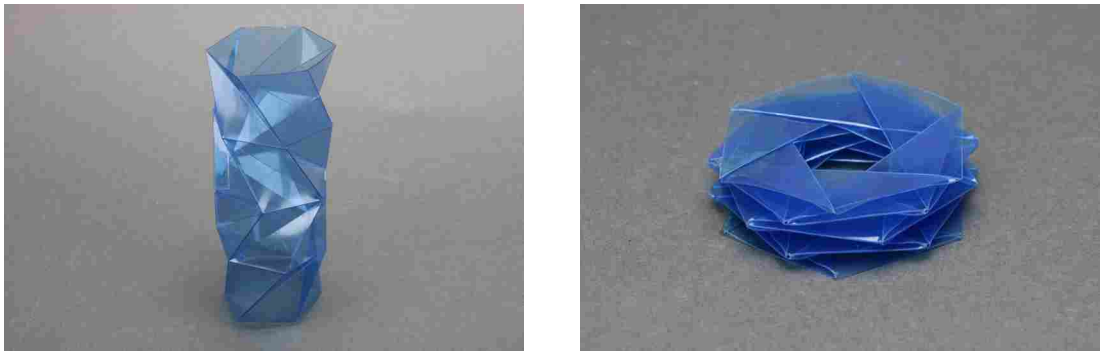

(a) Before heat set (b) After heat set

Figure 4.8: A Kresling pattern before and after heat setting treatment

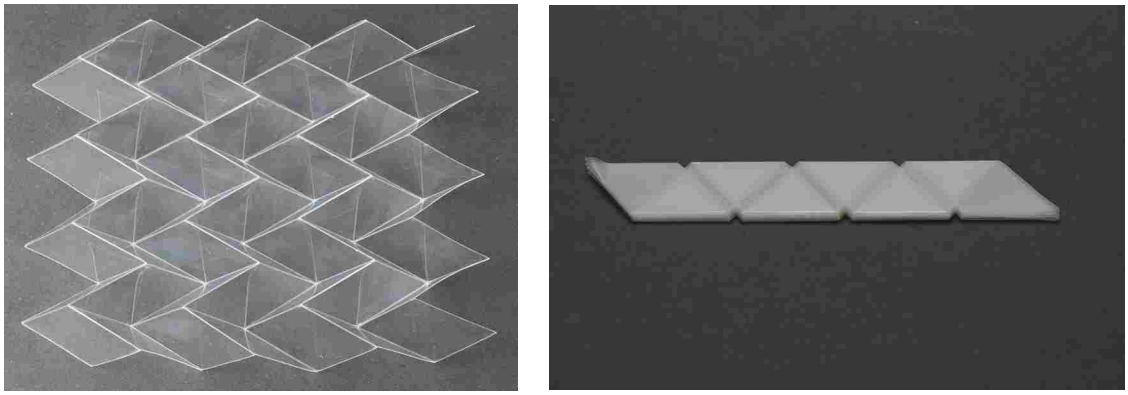

(a) Before heat set (b) After heat set

Figure 4.9: Miura-Ori tessellation before and after heat setting treatment in completely folded configuration

different applications, and elements of the pattern appear in many other patterns. It is also a rigid-foldable pattern, meaning that strain only occurs in the creases. The pattern was also used to again show the utility of the heat treating in creating patterns that will self-deploy from flat to folded.

The last pattern analyzed is the flasher pattern. This pattern was chosen due to the complexity and the deployed-to-stowed actuation. This pattern has been used in space solar arrays [28] where the pattern would be in the stowed configuration during transport and deployed in outer space. When folded in PET, the pattern tends toward the deployed position. The goal with applying the heat set was to see if the complex pattern would stay in the stowed configuration and return to that configuration after stretched to deployed and then released. The pattern was scored and folded and restrained in the folded state. After processing, the pattern remained in the stowed state

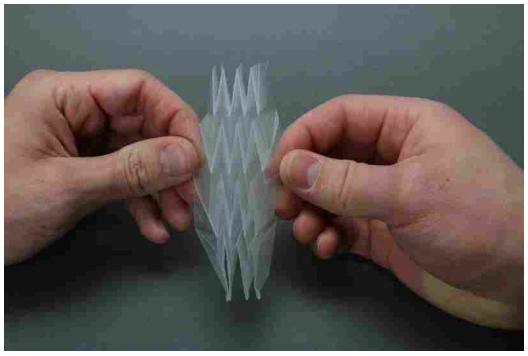

(a) Folded configuration

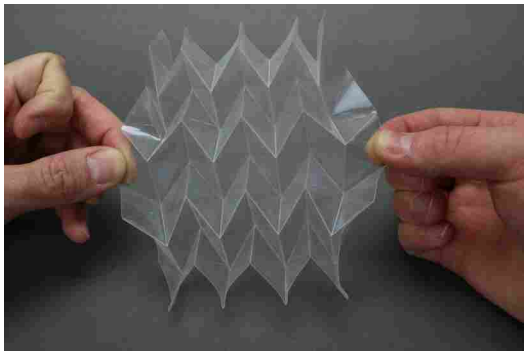

(b) Extending the pattern toward flat state

Figure 4.10: Heat set Miura-Ori tessellation through actuation

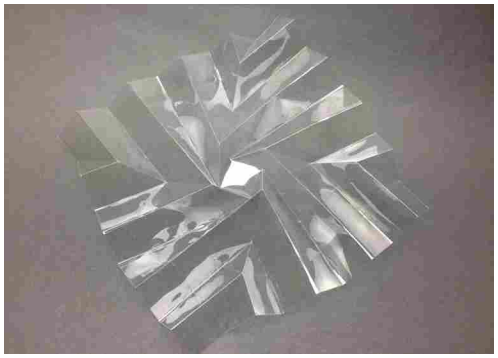

(a) Before heat set

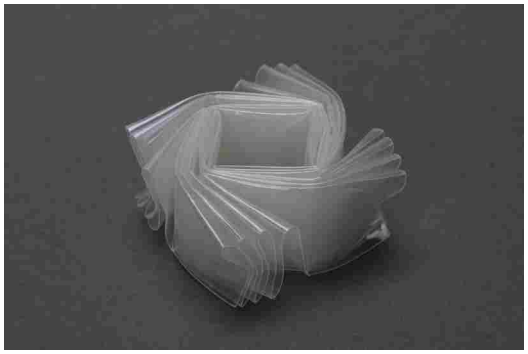

(b) After heat set

Figure 4.11: A Flasher pattern before and after heat setting treatment

after the restraints were removed. The pattern actuated smoothly to the extended state and snapped back to the folded position.

4.5 Potential Applications

Through the processing of the PET strips and origami patterns, we have shown that the polymer can be configured to have a position to which it will desire to return, even after actuation. This has multiple applications, including self-retracting mechanisms. When treated in the stowed state, as in the case of the Kresling and flasher pattern examples, the pattern can be extended to perform a function and then automatically retract to a stowed position for storage or transport. This tendency to bias towards the stowed position can also add tension into the pattern. Tension can be used for added stability of the mechanism. The added tension between the supports used to actuate

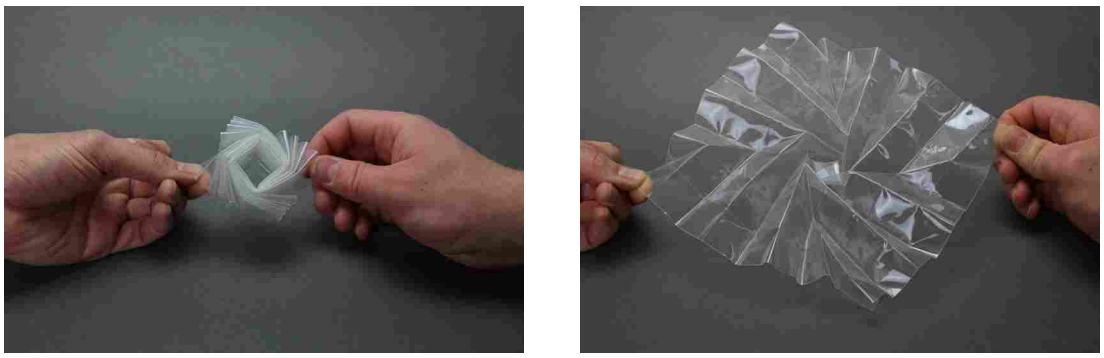

(a) Folded Configuration (b) Actuating toward extended state

Figure 4.12: A heat set Flasher pattern through actuation

the mechanism increases the stiffness. This can also be applied if the mechanism is designed to be in the deployed state for an extended period of time. The tension assists in making the pattern act more like a structure (as in a tensegrity structure where tension makes flexible members behave as rigid links).

This processing also has application in self-deploying mechanisms. The need for self-deploying mechanisms is common in many areas, from deployment of medical devices designed to enter the body in a compact configuration and deploy for use as in a heart stent to self-deploying shelters for quick set up. By processing the patterns into a folded or semi-folded state, it can be laid flat for storage or insertion and deploy to the desired state when the pressure is released.

4.6 Conclusion

Crystallinity has a large influence in the crease properties of PET film. Of the processing methods considered, temperature of processing was determined to be the primary factor in determining the force response. Models heated above the cold-crystallization temperature had a larger force response when stretched than those heated below T_c.

The force drop in the fold was insensitive to the processing methods considered. Therefore for those samples with higher force responses, the percent decrease was lower and the force response became the primary measure for how well the heating process assisted in holding a crease in the film.

The stiffness of the fold has been shown to be tailorable through heat processing. This can be applied to many origami patterns and origami engineering applications. Therefore PET can be tailored to the specific application desired. The treatment processes considered can provide a framework for others looking to find the optimal process for a given application.

CHAPTER 5. ZIPPER-TUBE REINFORCEMENT

5.1 Design Progression

5.1.1 Concept Overview

The Zipper Tube Reinforcement (ZTR) concept was inspired by a construction device, called a Buckling-Restrained Braced Frame (BRBF), used for support against seismic activity [29]. It works by supporting a center weight bearing column along the entire length while allowing movement of the center beam relative to the supporting walls. Other support systems, such as a pantograph/scissor mechanisms [3], only provide support at discrete stages. These discrete supports do not require changes to the center column but provide for additional axial load by adding lateral supports. This forces the interior beam into an increasingly higher buckling mode as shown in Figure 5.1. This helps avoid catastrophic failure and allows the beam to support a load even after multi-modal buckling.

5.1.2 Split-Tube Predecessor of the ZTR

A split polymeric tube was developed based on the BRBF concept. It is a simple design that illustrates some of the important issues and led to the ZTR. The tube has an inner diameter just larger than the diameter of the endoscope or catheter and envelops the device with a slit along the length of the tube. As the device is advanced into the body, the tube unrolls into a flat sheet and is spooled around a mandrel. This provides a compact storage for the tube. An advantage of this style of storage is additional length to the support system has a small effect on the overall system size. Other systems, such as a pantograph, require additional space for each additional support stage to fold and stack together. This limits the amount of support stages these systems can have. The number of parts also increases as more support stages are added. A single tube is easily cut to the length of the desired insertion stroke. As more material wraps around the mandrel, the mandrel

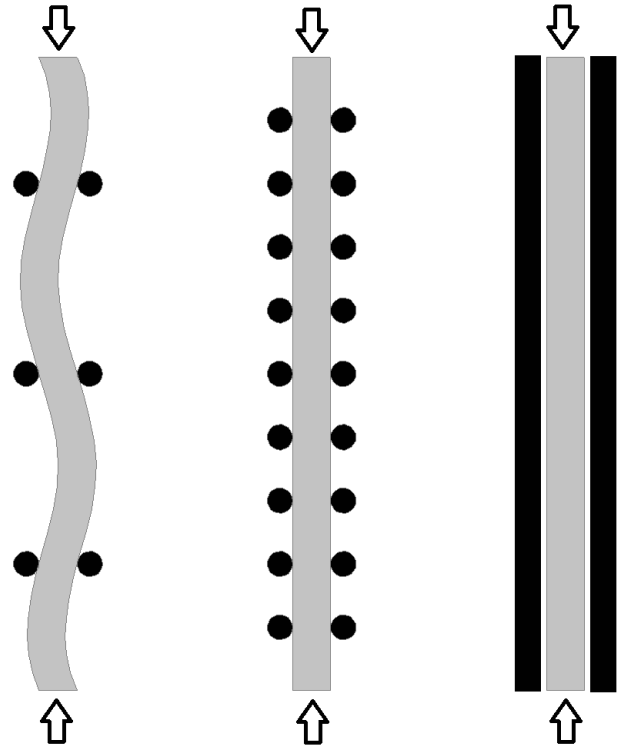

Figure 5.1: Concept of the BRBF transitioning from a standard support system like those used in a stage supported system (left) to adding more support points until it is supported along the entire length (right). The gray represents the catheter or endoscope and the black represents support points.

diameter increases, but the mandrel is set away from the tube insertion axis. This provides the ability to add length to the tube without increasing the collapsed size of the support system and therefore allowing for a large range of device lengths.

The split tube has an inherent defect such that upon buckling the catheter could eventually escape from the tube through the slit. Another problem was the stress relaxation of the plastic; the longer the plastic was left wound up on the mandrel, the less it would return to a circular cross-section, opening the slit more and increasing the likelihood of the device buckling out through the slit. Possible solutions were explored by introducing an overlap at the slit or having two tubes, one nested within the other with the slits offset by 180 degrees. These resolved much of the problem. However, these solutions significantly increased the complexity of the support system or manufacture while not completely resolving the issue presented by the slit.

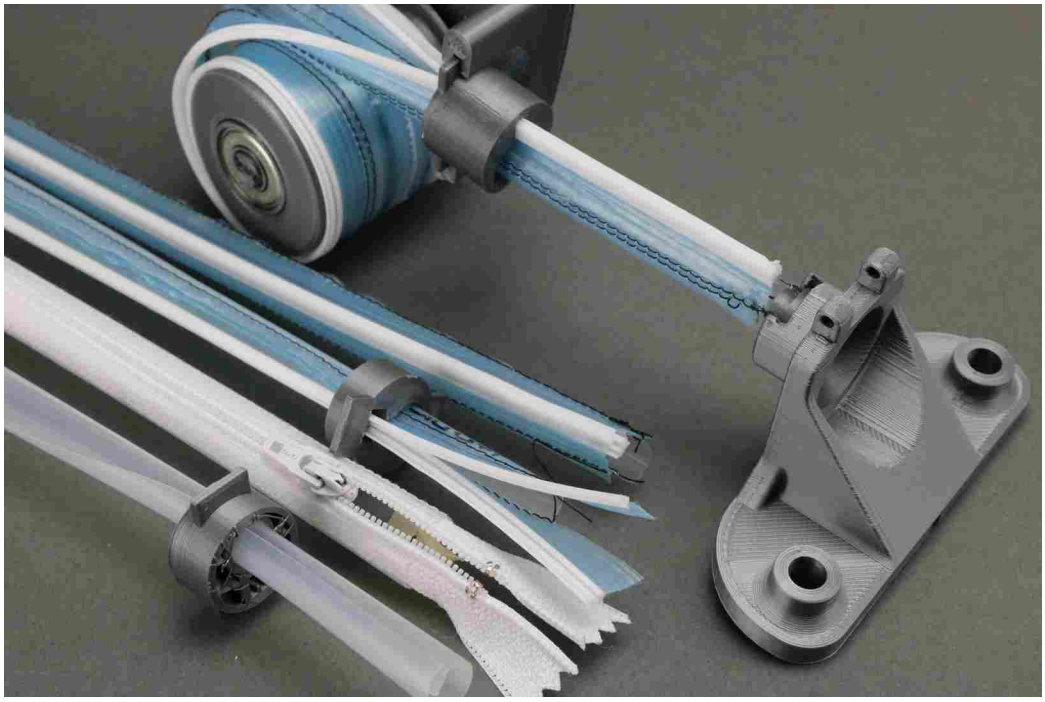

Figure 5.2: Tube concept progression with early prototypes on the left progressing to the final testing prototype on the right.

While studying retractable boom structures in spacecraft [30–32], it was discovered that placing a zipper on the tube resolved both the issues with stress relaxation and the escaping of the catheter while using one tube. Two styles of zipper were considered. The first is an end-to-end zipper, like those found in clothing. The second was a face-to-face zipper, like those used in sealable plastic bags. The face-to-face zipper was selected for prototyping as they could be integrated directly into the tube. Additional details on zipper selection can be found in the discussion of the tube components in the sections following.

Figure 5.2 shows a general progression from a single split tube to the testing prototype with a zipper. For prototyping and testing, the zippers were sewn onto the plastic tubing. Ideally the zipper and tube would be extruded as a single piece.

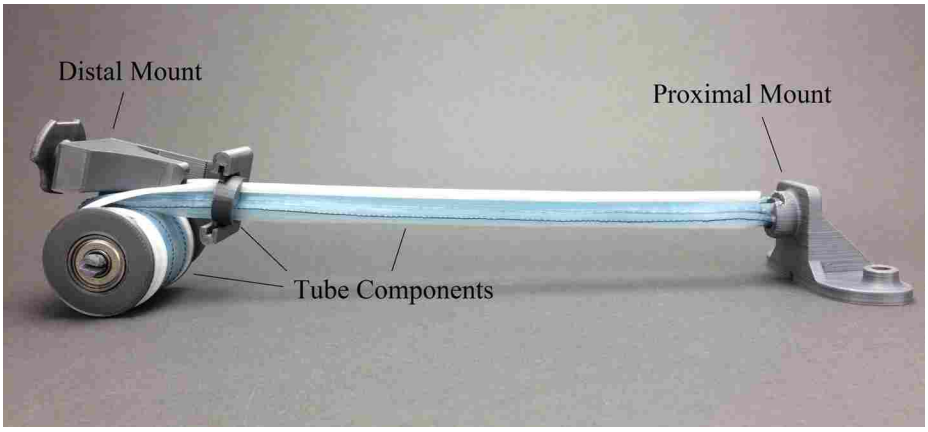

Figure 5.3: Full testing prototype with the three primary subsystems labeled

5.2 System Overview

The ZTR can be segmented into three basic subsystems: the proximal mount, the tube components, and the distal mount. A prototype showing all three subsystems is shown in Figure 5.3.

5.2.1 Proximal Mount

The proximal mount is designed to be the mounting closest to the robot body. It serves only as a connection for the tube end to the robot and the location that the catheter or endoscope would be mounted. The catheter would travel from the proximal mount through the tube to the distal mount and from there into the patient. It should be noted that the design for the proximal and distal mounts can easily be switched. This setup was chosen because if the mandrel is placed on the proximal mount, the tube moves relative to the device, introducing additional friction and wear on the device. This is eliminated if the mandrel is placed on the distal mount.

In the current design, a slot was added so that the tube end, fitted with a mating adapter, could click in and out of place (See Figure 5.4). This allows the tube to be easily loaded and removed with no additional parts. The tube can also be top loaded. Other tube attachment methods could be used.

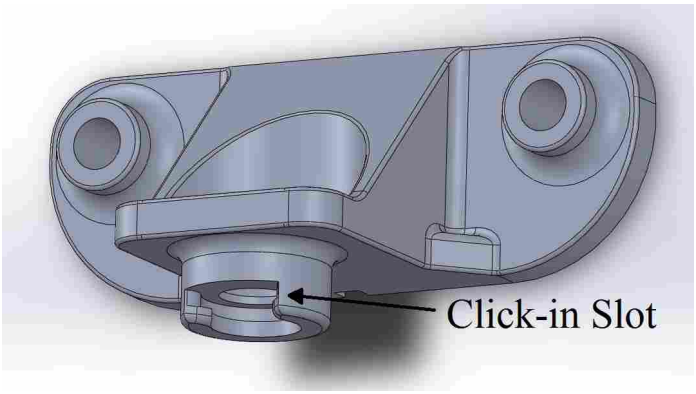

Figure 5.4: CAD drawing of the testing proximal mount with the tube click-in slot labeled

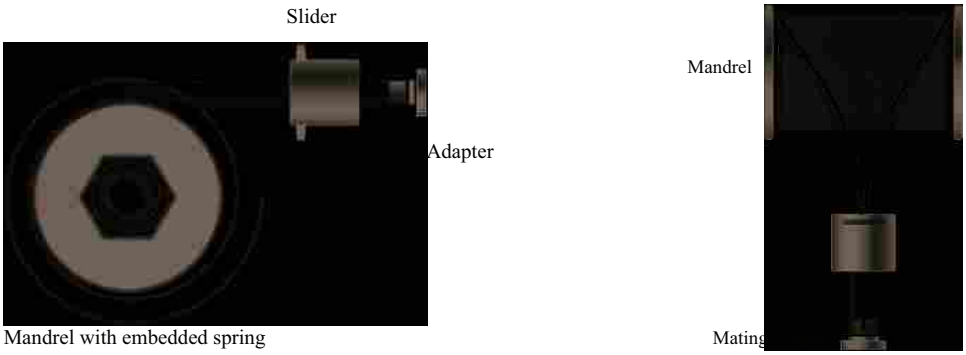

(a) Side View (b) Top View

Figure 5.5: Concept drawings of tube components subsystem. The black parts could be injection molded parts with the clear segment being the extruded polymeric tube with the zipper.

5.2.2 Tube Components

The tube components consist of four parts and can be designed to be single use. Figure 5.5 shows a concept drawing of these parts together as a unit. Figure 5.6 shows the subsystem used in the testing prototype. This design is composed of the tube, the mandrel that the tube wraps around, a mating adapter adhered onto the proximal end of the tube for attachment to the proximal mount, and a slider that would mate and separate the zipper segment of the tube. The design of this slider is made to be attached to the distal mount and guide the tube into a circular shape. It functions similar to a face-to-face zip slider on a slider sealed plastic bag. In prototyping, 24x20” Jumbo Slider Zip Bags from ULINE were used.

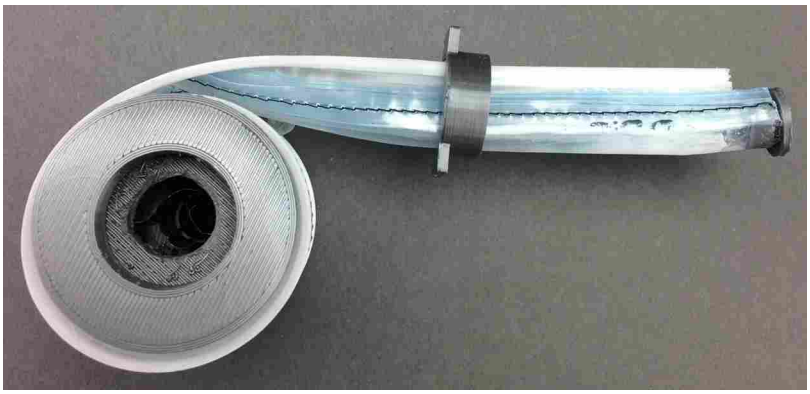

(a) Side View

(b) Top View

Figure 5.6: Physical prototypes of tube components subsystem shown in Figure 5.5

Using the face-to-face zip sliders, the tube naturally forms a tear-drop shape. While this shape performed well compared to a circular cross-section, it lowered the lateral stiffness of the tube as the cross-sectional moment of inertia is lower in the direction perpendicular to the zipper, biasing the tube to bend and buckle in that direction under a compressive load. A shape with a radially constant moment of inertia would eliminate this and therefore create a higher overall stiffness. Figure 5.7 shows examples of the three cross-section types considered using the plastic zipper segment from the slider zip bags. The difference comes in where the tube connects to the zipper segment. As the cross-section approaches a circular shape, the moment of inertia will approach a constant value radially. The design needed to make the slider for the overlap cross-section is more complex as is requires a free hanging member inside the tube to mate the zipper. Configuring an end to end zipper such as those in clothing zippers would eliminate the overlap and additionally assist in approaching a circular cross-section. Preliminary designs for these slider types have been created and the tear-drop configuration was used in the testing and prototyping reported here.

The mandrel is made to roll on an axle attached to the distal mount. The mandrel houses a constant force spring embedded inside such that the spring would be in its natural state when the tube is completely wound around the mandrel. Therefore, as the tube is extended, the spring would be extended and the force exerted by the spring would put the tube in tension. This is important for two reasons. First, this aids in auto-retraction of the tube and ensures a tight spooling of the tube around the mandrel. Second, the tension in the tube eliminates the risk of the tube itself buckling.

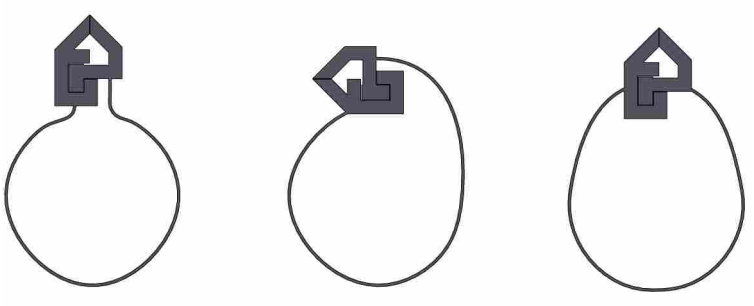

Figure 5.7: Sketches of three different zipper tube cross-sections, from left to right: tear drop, overlap, end-to-end

As the mandrel auto-retracts the tube, no compressive loads are applied to the tube as the robot arm is actuated.

5.2.3 Distal Mount

The primary functions of the distal mount are to connect to the distal arm of the robot and provide for spooling and stowing the tube in the rolled configuration.

In this design, the mandrel slides onto a fixed shaft in the distal mount and the spring attaches to the shaft such that as the mandrel rotates, the spring deflects, creating the force for tension in the tube and auto-retraction. Other retraction methods, such as a motor, could be integrated into the distal mount and remove the need for a spring but this adds complexity in requiring additional power and programming. For ease of manufacture, the spring in the tube components was used in prototyping.

A concept drawing of the full system is shown in Figure 5.8. Design concepts envision a casing around the mandrel to protect the tubing from pathogens and improve aesthetics.

5.3 Modeling

A simplified model was created to better detail material selection on the performance of the system and to characterize the forces required for actuation in order to optimize the design. This modelling focused on the interface of the tube with the slider and the corresponding forces applied by the slider on the tube to roll the tube from the flat configuration to a rolled-up and zipped

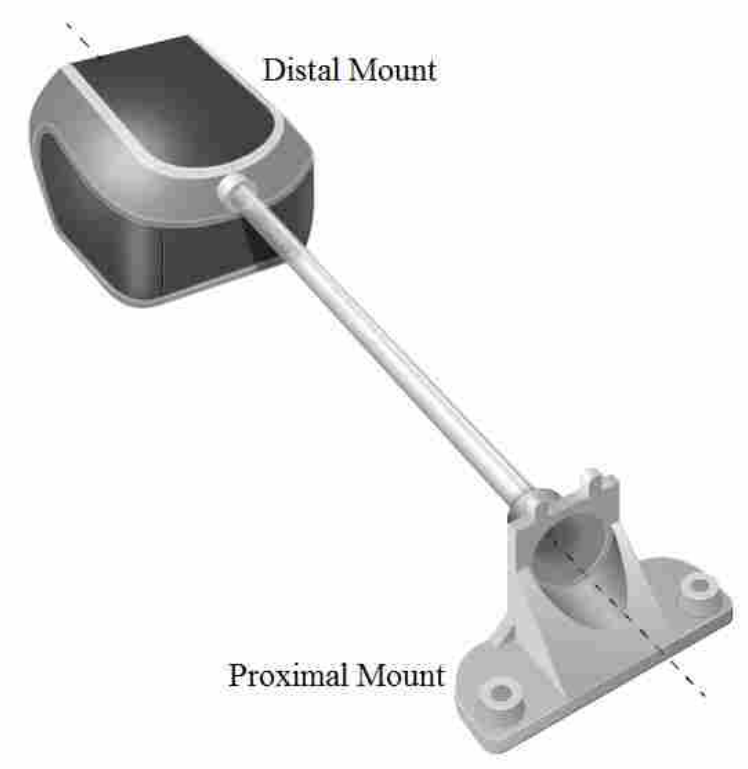

Figure 5.8: Concept drawing of full ZTR system

tube. This was chosen as once the tube is rolled into a circular configuration and zipped closed, the zipper will provide the force required to keep it in the circular configuration. When wound around the mandrel, the tube is in the flat state which due to the stress relaxation discussed above will likely be its stored state. The winding method- a constant force spring or motor, will keep it tightly wound around the mandrel. Therefore, the area of greatest interest is the transition of the tube from the flat state to the rolled-up and zipped state and vice versa. This is where the primary source of actuating friction occurs. This happens in a relatively small transitioning area between where the tube leaves the mandrel to where it exits the zipper mechanism (approximately 45 mm in the prototype).

To model this motion, only the length of the tube in this transition area was considered. Two models were devised using the cross-section of the tube as the geometry and the length of the transition area as the out-of-page width: a pseudo-rigid-body model [4] of a cantilever beam with an applied constant moment load to model the tube cross-section as it moves from a flat state to a rolled-up tube configuration (Figure 5.9a), and a pseudo-rigid-body model of the zipping segment

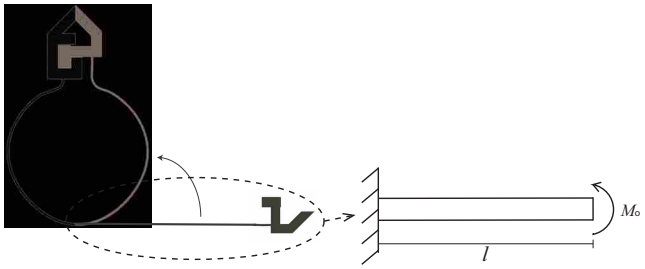

(a) Tube modeled as a fixed-free beam

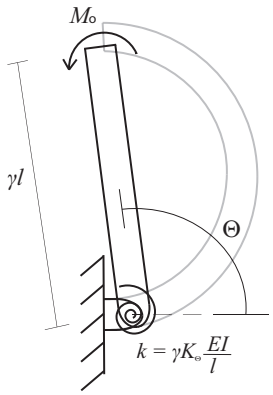

(b) Pseudo-Rigid-Body Model of tube model with the compliant mechanism in gray

Figure 5.9: Modeling used to predict the force required to deflect the tube into a circular configuration

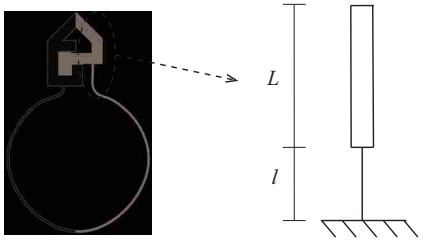

(a) Zipper segment modeled as a rigid segment attached to a flexible segment

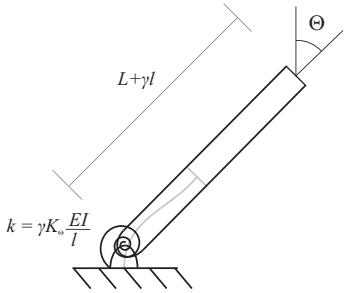

(b) Pseudo-Rigid-Body Model of zipper model with the compliant mechanism in gray

Figure 5.10: Modeling used to predict the force to deflect the zipper segment during mating of zipper segments

on the tube as a rigid segment on a flexural pivot to model the required displacement load to mate and unmate the zipper (Figure 5.10a). By modeling the forces in this area, the frictional forces can be predicted.

The tube model assumes symmetry along the midline of the flattened tube and therefore models the tube cross-section as a fixed-free beam with half of the width of the flattened tube as its length. A constant moment load is chosen to model the circular curvature of the tube once the zipper is connected. The model also assumes that the plastic's equilibrium state is flat. This was chosen as the tube will likely be stored flat and spooled on the mandrel before use. This model

predicts the normal force from the tube as it attempts to return to a flat state. This force would be held by the zipper segment in the tube section but translates to friction against the zipper on the proximal mount during the zipping motion. This normal force is estimated below.

Once the tube is rolled into a circular configuration, the two zipping segments for the face-to-face zipper still have to bend away from each other in order to mate easily. The force to connect the two zipper halves is resultant of a displacement load to bend one half of the zipper. An angular displacement of about 45^o was is needed to mate and unmate the zipper. This was modeled as a rigid segment (the zipper segment attached to a thin 0.127 mm stem below the zipper head (the tube). The model and its accompanying pseudo-rigid-body model are shown in Figure 5.10. The zipper model assumes that parallel segments of interest are compliant and the remaining segments, comparatively, are rigid. Initial inspection of the motion of the zippers revealed that this assumption closely models the motion of the plastic zipper. With this model, the zipper components nest within each other in an equilibrium position. The creep that the tube introduces in this zipper state is small enough to be ignored. The force needed to move the zipper segment in and out of its deflected state to mate and unmate the segments translates to friction against the zipper. Combining the equations from the two pseudo-rigid-body models predicts the total normal force needed to be applied by the zipper to mate and unmate the zipper segments.

Normal forces required to keep the tube in a circular configuration were estimated as the force to keep the psuedo-rigid-body model in Figure 5.9b in the deflected position shown. This is represented by

$$FL = k\Theta \tag{5.1}$$

where

$$L = l\gamma \tag{5.2}$$

l is the length of the compliant beam, therefore half of the width of the flattened tube. For a fixed-free beam under a constant moment

$$k = \gamma K_\Theta \frac{EI}{l} \tag{5.3}$$

where $K_\Theta = 2.064$ and $\gamma = 0.735$. Therefore

$$F = \frac{K_\Theta EI}{l^2}\Theta \tag{5.4}$$

E is the elastic modulus of the material and I is the moment of inertia. The beam was modeled as a rectangular cross-section, $I = \frac{bh^3}{12}$, where b is the length of the transition area and h is the material thickness. For the beam to bend to a half circle, the end angle, θ_o, would need to deflect to $\theta_o = \pi$. For fixed-free boundary condition under a constant moment,

$$\Theta = \frac{\theta_o}{C_\Theta} \tag{5.5}$$

where $C_\Theta = 1.5$. As the results found in Eq. 5.4 only represent half the tube, the full force of bending the tube would be

$$F = 2\frac{K_\Theta EI}{l^2}\Theta \tag{5.6}$$

For the prototype system ($b = 45\,mm$, $h = 0.127\,mm$, HDPE $E = 0.8\,GPa$, $l = 12.5\,mm$), 0.34 N was estimated to keep the tube in a circular configuration.

For modeling the deflection of the zipper segment during mating and unmating the zipper segments, the psuedo-rigid-body model in Figure 5.10b was modeled as undergoing a deflection of $\theta_o = \frac{\pi}{4}$. This was modeled as a rigid segment attached to a flexible pivot. As the rigid segment is so small, it was determined not to model as a small-length flexural pivot but as a flexible beam with the same end angle as the rigid segment. This yields equations for the force identical to those found in the first model, the force needed to deflect the two segments found using Eq. 5.6. The difference is in this case $\gamma = 0.85$, $C_\Theta = 1.24$, $K_\Theta = 2.65$ and l is approximately half the length of the rigid segment. Adding the forces from the two models together results in an estimate of the normal force applied by the zipper on the tube to mate and unmate the tube zipper segments.

For the prototype ($l = 1.27\,mm$), 12.79 N was estimated to keep bend the zipper segments. Adding that to the force found in the first model results in a total normal force of $F_n = 13.13\,N$. The friction can be determined by

$$F_{fric} = \mu F_n \tag{5.7}$$

for plastic-plastic $\mu \approx 0.4$ for dynamic friction [33], therefore, 5.25 N frictional force caused by the zipping motion. Additional friction could come in the rubbing of the tube on the walls of the zipper. This frictional force is much harder to model and would have to be determined empirically.

Using this model, the force to actuate the zipper along the tube can be estimated for any given tube geometry and material and aid in the design of zipper designs. The frictional forces encountered in the tube-proximal mount interface during zipping add to the load needed by the constant-force spring for auto-retraction or torque of the motor, depending on selected mandrel winding method. Both drawing or retracting the tube mechanism are affected by these forces and have to be quantified to determine the constant-spring force required (for using spring driven), the actuation force required to draw out the tube, and the geometry of the proximal mount at the zipper connection site.

5.3.1 Tube Material Selection and Manufacture

To optimize the system performance, an analysis of the material properties on the previously modeled forces was conducted. The tube and zipper could be extruded in one solid piece, with many polymer options available. Polymer tube extrusion is well suited for large quantities and would assist in making the ZTR a partially disposable system. Single-piece extrusion would result in lowering the friction of the zipping motion and would lower the actuation force required. Tubes investigated were constructed from PET, LDPE, and HDPE, all of which showed promise as a final product but material selection is not limited to these materials alone. The differing material properties of these plastics lead to different normal forces for actuation and deflection of different segments within the tube. for example, using the model of the zipper segment, the predicted force to deflect the zipper segments as a function of Θ for various polymers are shown in Figure 5.11. Polymers with a lower force to deflect would reduce the friction in the zipping motion and assist in auto-retraction, but would also reduce the lateral stiffness of the tube.

5.4 Testing

Testing was performed to measure how much of a compressive insertion load a device within the support system could undergo before buckling. For both tests, a 4.5 mm diameter artic-

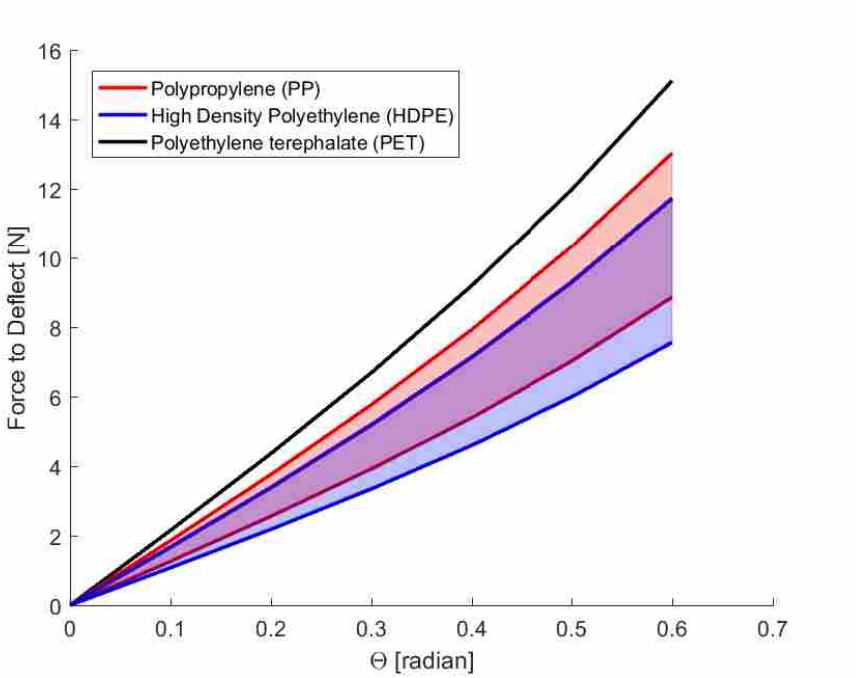

Figure 5.11: Modeled forces to deflect zipper segment for different polymers

ulating catheter used in robot-assisted lung biopsies was used as the example device. The first test, a static test, was designed to observe the amount of load the catheter itself could undergo while in the support system. This was done by deploying the system to a set of fixed lengths and adding a compressive load on the catheter on the distal end. The load was increased until the device would no longer support the load (buckling failure) or the device failed in such a way as to damage the device (e.g. kinking or crushing). The set of lengths was measured as the amount of exposed tubing between the proximal and distal mounts; therefore fully inserted is 0 m. For the test set up, the fully retracted position resulted in a 0.4-0.5 m distance between the proximal mount and the distal mount. The set included 5 mm increments until the load began to crush the catheter rather than buckle. Results for this test are found in Figure 5.12.

The second test, a dynamic test, was to apply an insertion load to the catheter and the system jointly from the proximal end. The catheter would be held fixed at the distal end. The tests started at the same set of fixed lengths as in the first test and the proximal end would advance from that point until buckling commenced. The force applied to the proximal end at that set was measured, subtracting out the force required to actuate the support system without the device. The

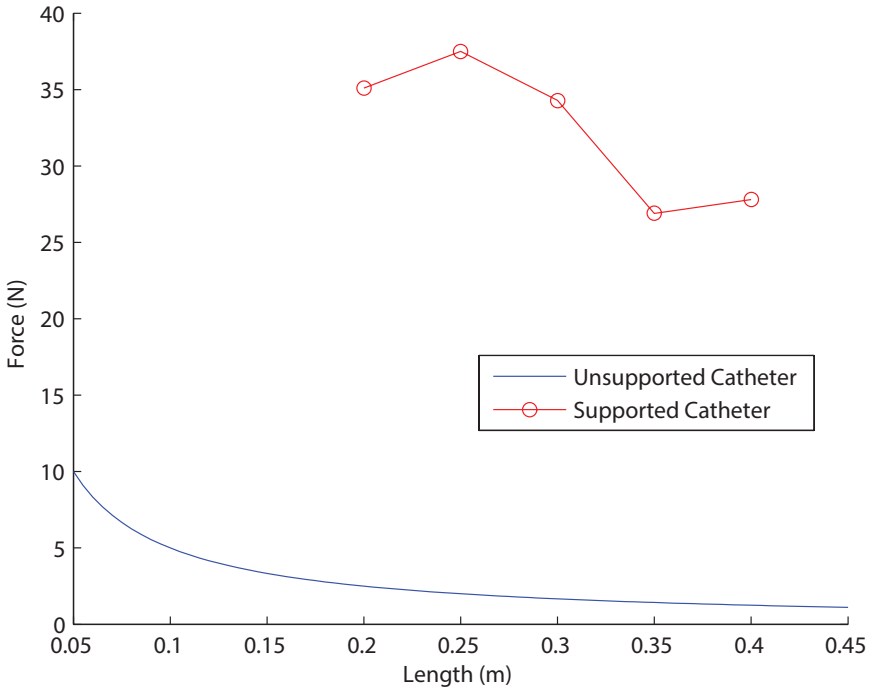

Figure 5.12: Results of the static test comparing to unsupported catheter

system was then advanced to the next starting length in the set. This translates into the amount of force a robot can apply to the device at a given insertion length before the device would fail in buckling should the device meet resistance during insertion. Results for this test are presented as a set of points representing the maximum force before buckling, P_{crit}, for a given insertion length starting length. Results for this test are found in Figure 5.13.

The prototype used a 0.127 mm-thick tube of HDPE with a constant-force spring of approximately 5 N to counteract the insertion friction. This resulted in a force to extend of about 13 N and about 1.5 N to insert without the device present. Compressive tests on this catheter resulted in a trend of

$$P_{crit} \approx \frac{1}{2L} \tag{5.8}$$

where L is the length between the fixed ends.

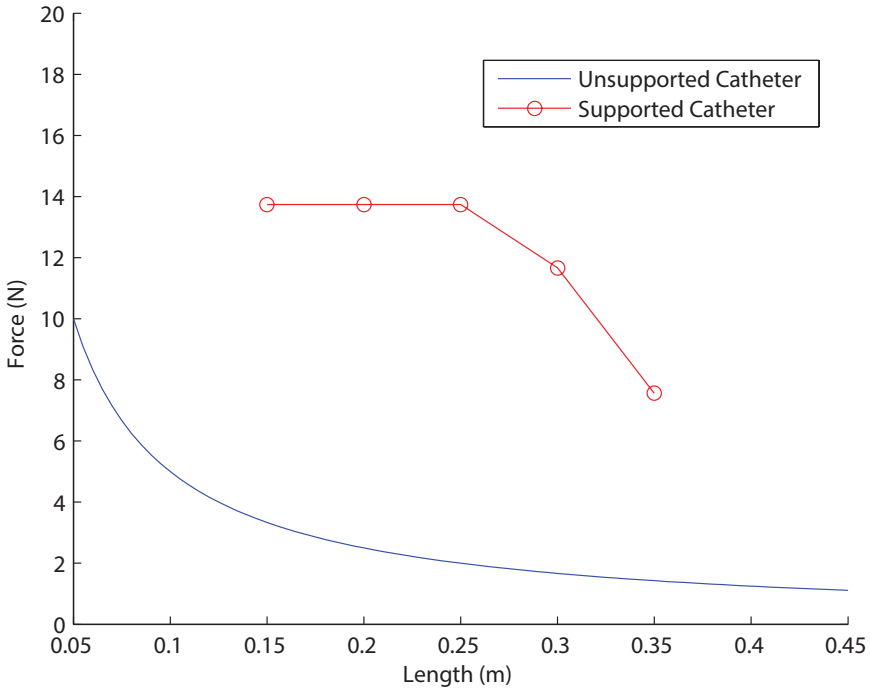

Figure 5.13: Results of the dynamic test comparing to unsupported catheter

5.5 Discussion

5.5.1 Test Results

The results from the static test procedure showed an increased critical load supported by the catheter while in the ZTR system. When fully retracted the catheter could support over 25 N more than the catheter could support on its own. This support system made it almost impossible to buckle the catheter at lengths less than an insertion length of 0.15 m, the catheter beginning to crush instead. It is assumed that the robot system would never apply this high of a load as it could injure the patient or the device. Therefore, the catheter is completely supported for the operating range of the robot. In observing the test, the catheter would buckle within the tube in a multimodal state as predicted, then with increased loading, the catheter would eventually transfer enough of a load to the tube wall to bend it out. This essentially applied a lateral load to the tube from the interior. Increasing the thickness of the tube or the tension provided by the constant-force spring would increase the lateral stiffness of the tube.

In the dynamic test, the ZTR system increased the critical load by about 10 to 12 N. As in the static test, the catheter buckled inside the tube. A small amount of friction was still unaccounted for by the constant-force spring, therefore some of the actuation loading was transferred to the tube. Due to this additional force, the force is lower in the dynamic test compared to the static test. If the tube was in higher tension through lower friction or a stiffer constant-force spring, the tube could auto-retract more freely and the tension in the tube would increase its stiffness. Higher tension would increase the force to extend the tube, therefore work to reduce the friction would be the first approach. One solution to reduce the friction would be to add two rollers to the sides of the proximal mount that press the zipper together. This solution will remove the majority of the dynamic friction between the tube zipper segments and the proximal mount.

5.5.2 Enabling Features

ZTR systems have several features that could enable further developments and improvements to the robot surgical systems and operations. Primary among these is the ease with which these models can be changed to accommodate other catheter sizes. The ZTR could be tailored to a differing D_i by changing the extrusion pattern and adapting the other tube components to the new diameter. Because the ZTR provides a continuous support of the catheter, it could be used for thinner and more flexible devices. This could allow for more surgical procedures or greater access using current procedures. It also performs well when a force is added directly to the catheter and therefore could be used for catheters in different applications requiring more direct force to the device.

The ZTR also seals the catheter and therefore protects the catheter from external contamination, external damage, and prevents any biomaterials or other contaminates from coming from the catheter and entering the room or robot system. This is an attribute not exhibited by current anti-buckling guides.

The ZTR concept could also be modified to provide for a top-loaded catheter robotic system. In this way, the catheter would not have to be threaded through an anti-buckling system but could be loaded from above. In the current state, the ZTR already allows for the catheter to be inserted at any position of the robot arm where most anti-buckling systems require the system to be fully compressed before the catheter can be inserted.

5.5.3 Other Applications

ZTR systems could also find application in other areas. The ZTR is naturally a deployable boom structure. This could find application in space applications, other surgical instruments, or deployable booms for mics or cameras. It is also a deployable closed tube. This could be used in a variable length delivery system for fluids or soft materials. The protective feature could also find application in deployment of a protective sheath over cylindrical components, such as wiring, that could easily be retracted for maintenance.

5.6 Conclusion

The continuous support of the ZTR system enables variable-length devices to undergo much higher compressive loads before failure. This proves to be an effective support system for devices undergoing a compressive insertion force. It also provides additional enabling features that can expand the surgical field and enable other uses for the support system.

CHAPTER 6. RETRACTABLE SUPPORT SYSTEMS

6.1 Conceptual Development

Buckling failure can occur when a compressive force is applied to a structure. The basis of the systems presented in this work focus on avoiding buckling of a flexible device by supporting it with a system that is in tension. Some mechanisms that are required to undergo compressive loads invert the load to a tensile loading to avoid failure due to buckling [34]. Along with avoiding buckling, a structure in axial tension undergoes stress stiffening becoming more stiff laterally. The greater the tension in the system, the more laterally stiff it becomes. For a collapsible system, an example to understand lateral stiffness due to axial tension is an extension spring. A spring with a high spring constant has a greater lateral stiffness as it is extended when compared to a spring with a lower spring constant. Additionally, through the stroke of an extension spring, the spring never goes into compression and therefore will never buckle during actuation. Applying this principle to collapsible support structures, a system with high tension through the stroke will provide a more laterally stiff support structure. The flexible device can be connected to the support structure at discrete support points built into the support structure. The addition of support points will force a buckling member into a higher buckling mode (see Figure 6.1). Using Euler buckling, the critical force a long, slender member can withstand before buckling, P_{crit}, is a function of the length, L, between the supports squared:

$$P_{crit} = \frac{\pi^2 EI}{(KL)^2} \tag{6.1}$$

where K is a constant determined by the boundary conditions ($K = 1$ for pinned-pinned boundary conditions). If the device and boundary conditions remain unchanged, the buckling equation becomes a function of only L. Therefore, for evenly spaced supports P_{crit} for the entire device increases by a factor of $(n+1)^2$ where n is the number of supports. Through the integration of

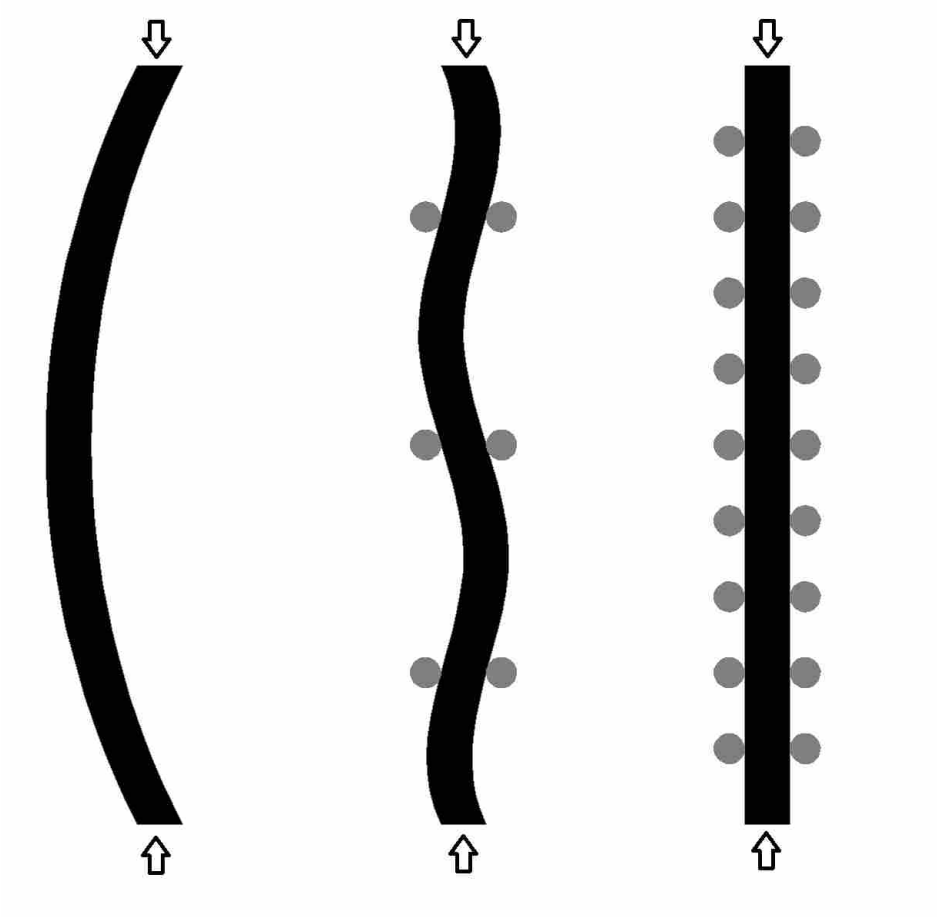

Figure 6.1: Under a compressive load, additional supports will force a buckling member into a higher buckling mode increasing the load capacity of the member. Supports are shown in gray with the flexible device in black.

discrete support points in collapsible systems, two support systems have been developed: “Wires in Tension” and “Orthogonal Beams”.

6.2 Wires in Tension

The Wires in Tension concept was developed to minimize the operating volume of the device. As pantograph systems collapse, like that shown in Figure 1.2, the rigid links change orientation requiring more volume laterally. In the Wires in Tension concept, two wires run in parallel to the flexible device (see Figure 6.2). The wires are put in tension to add lateral rigidity to the wires. The wires are spooled around a mandrel during the insertion stroke providing for tension

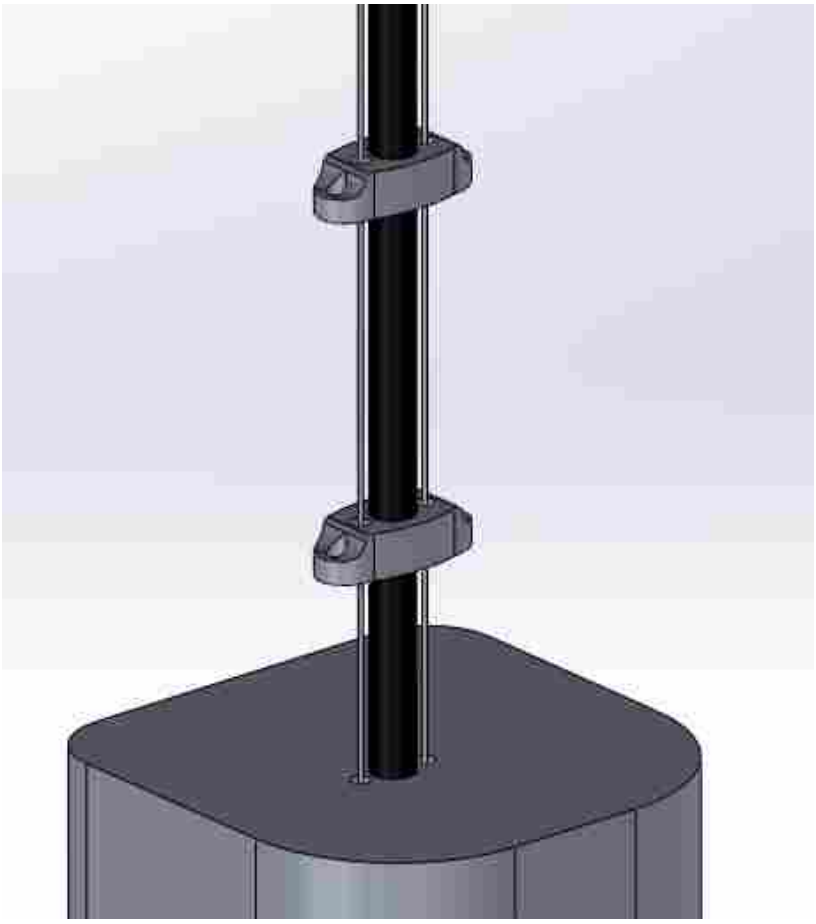

Figure 6.2: Wires in Tension concept: the support system, shown in gray, features two parallel wires held in tension, and two sliders are shown which provides support points for the flexible device, shown in black.

in the wires and a collapsible system. The mandrel could be either actively or passively wound. Active winding would involve a small motor to maintain the tension in the device retracting the wires proportional to the amount of insertion of the robot. A passively wound mandrel maintains the tension through the deflection of a constant force spring. At the fully inserted position, the spring would be in the undeflected state. Through the stroke, the spring would deflect and add a torque to the mandrel that would translate into a tension in the wire.

Support points are added through small sliders. These sliders move freely along both the flexible device and the wires. The thickness of the slider is determined by the diameter of the device. When the slider are at least as thick as the diameter of the device there is a reduced chance of binding while sliding along the device. The sliders are connected to each other by a separate

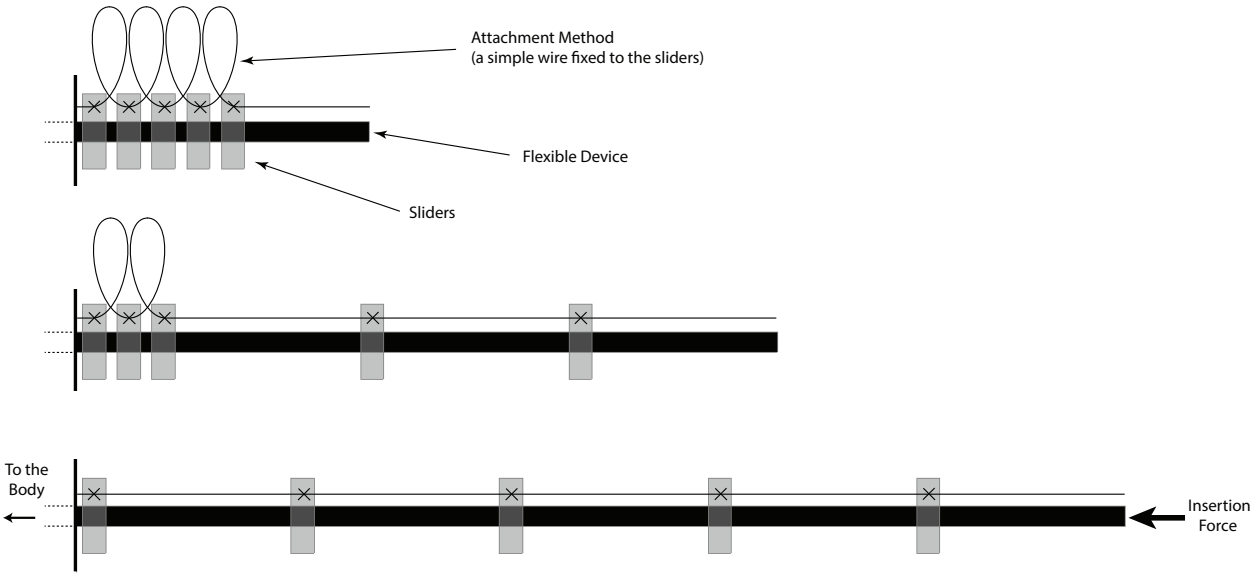

Figure 6.3: Motion of the support sliders, shown in gray, through three stages of insertion. The top represents near full insertion, the middle is partially inserted, and the bottom shows fully extended position. The flexible device is shown as the thick black line. The thin black line represents the attachment method to constrain the sliders to an even maximum spacing through the stroke.

wire with a fixed length between sliders. This provides for the sliders to be evenly spaced at full extension and that at no point during the stroke is there more than the fixed length between supports (as shown in Figure 6.3). Depending on the spacing required, other forms for spacing the sliders could also be conceived (e.g. small extension springs between sliders, magnets with like poles on each slider to repel each other, etc.). For evenly spaced sliders, the number of sliders for a given stroke length determines the spacing. The number of sliders and the width of each slider determines the minimum dimension along the insertion axis of the support system in the fully compressed state. The more the insertion axis dimension can be minimized will also minimize the amount of the device that is unusable. The dimension of the support system radially out from the device is determined by the size of the support sliders. As opposed to a pantograph system that widens radially as it compresses, the wires in tension system does not change in size during the stroke, reducing the operating volume of the device.

6.2.1 Actively Wound

Two winding systems can be used to draw in the wires and maintain tension in the wires. The first, the actively wound system, would use a motor to drive the mandrel. The motor would be programmed to turn in proportion to the amount the robot arm advances while keeping a preset amount of tension in the wires at all times. The preset amount of tension is determined by the allowable force the motors can sustain. This method provides for a constant tension in the wires and provides for a maximum tension in the wires proportional to the torque of the motors used. For a non-back-drivable motor used for winding, the motor would resist any extension of the wires caused by lateral deflection. Therefore, the lateral stiffness in an actively wound system could be high while transferring minimal additional tensile load to the robot. However, this style requires an additional motor and programming to function.

6.2.2 Passively Wound

To reduce the need for additional instrumentation, a second winding method was developed. The mandrel is actuated by a constant-force spring, with the undeflected state being the fully wound position. As the support system is actuated, the constant-force spring is deflected and provides tension to the wires. This method is less complex than that of the actively wound system but because the lateral stiffness is a function of the spring stiffness, the robot will be required to resist the full tensile load in the wires caused by the spring. Higher tensile loads are preferred for greater lateral stiffness but high loads on the robot arm could have adverse effects on the motors driving the robot arm. Therefore the maximum tension in the wires is largely determined by the amount of force provided by the motors driving the robot arm.

6.2.3 Modeling of Lateral Stiffness and Tension in Wires

The tension required for a desired lateral stiffness is modeled in the following manner. When the device buckles in the first mode, it will add a lateral force, F_{lat}, primarily on the center support slider. This force will cause the slider to displace laterally, δ. This is depicted in Figure 6.4a. For a passively wound system, tension applied in the wires, T, is a function of the constant-force spring constant, K_t, and the radius of the mandrel, r, yielding the relationship

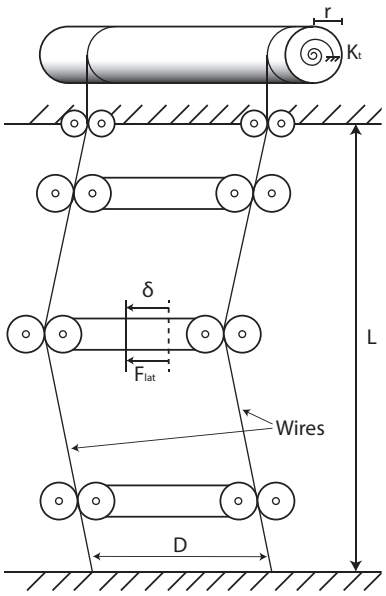

(a) Illustration of the passively wound Wires in Tension model with three support sliders. A lateral force, resulting in a lateral displacement, is applied on the middle of the support slider.

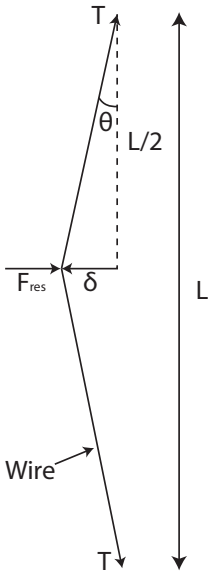

(b) Free-body diagram of the wire

Figure 6.4: Modeling of the Wires in Tension concept

$$T = rK_t \tag{6.2}$$

L in Figure 6.4 represents the distance between fixed points. In robot systems, the fixed points are the proximal and distal mounts of a robot arm which actuate relative to each other as the device is inserted. Therefore, L will change throughout the insertion stroke. For a given value of L, a free-body diagram of the wire will reduce to Figure 6.4b.

From the free-body diagram, the restoring force, F_{res}, can be calculated by

$$F_{res} = 2Tsin(\theta) \tag{6.3}$$

$$tan(\theta) = \frac{\delta}{L/2} \tag{6.4}$$

Using small angle assumptions $sin(\theta) \approx \theta$ and $tan(\theta) \approx \theta$, therefore

$$F_{res} = 2T\theta \tag{6.5}$$

and

$$\delta = \frac{L\theta}{2} \tag{6.6}$$

Combining eqns. 6.5 and 6.8 yields

$$F_{res} = \frac{4T\delta}{L} \tag{6.7}$$

As F_{res} is a function of the deflection, it will continue to increase until it becomes equivalent to F_{lat} at which point the system will no longer deflect. Therefore, the deflection as a function of the lateral force can be written as

$$\delta = \frac{F_{lat}L}{4T} \tag{6.8}$$

This model requires an estimate of the lateral force applied by a device buckling in the first mode as a function of the length between supports and the axial force applied to the device. This model assumes the lateral force will act primarily on the middle slider and that the middle slider is set at the length $L/2$. It also assumes the number of sliders is sufficient such that the device buckles in the first mode rather than a multimodal buckling failure as in the middle image in Figure 6.1. In multimodal buckling, L changes to the length between supports and Eqn. 6.1 is used to predict the axial force the device can withstand before buckling.

For actively wound systems, the tension in the wire is an addition of force required to back-drive the motor and how much preset tension the motors apply to the wires. Therefore, as this tension could be significantly higher than that of the passively wound system, the restoring force for actively wound systems would be much higher than that of a passively wound systems.

As the simplicity of the passively wound system can be desirable, further research led to a variation of the wires in tension concept to increase the lateral stiffness while allowing for a passively wound system. This research led to the Orthogonal Beams concept.

6.3 Orthogonal Beams

The Orthogonal Beams concept is similar to the Wires in Tension through putting two long members in tension and sliding support points along the length of the tension members. The Orthogonal Beams concept gains additional stiffness by placing two thin strips orthogonal to each other in place of wires. As a load is applied in one direction, the strip that is parallel to the direction of the force will provide the primary source of lateral stiffness as the area moment of inertia of the strip cross-section will be very large where the other strip adds little to the stiffness. For a load that is applied that is not parallel to either of the strips, both strips contribute to the stiffness, therefore enabling a system that will resist bending from loads applied in any direction. The strips are held together by small sliders as in the wires in tension that provides a hole for the catheter to pass through, as shown in Figure 6.5. This concept could be actively wound, but as it was developed primarily to increase stiffness in passively wound systems, passive winding will be considered. Passive winding could be accomplished by having a flat strip on a mandrel and a constant-force spring at one attachment point on the robot as in the wires in tension or actually using the constant-force spring as the strip itself. Constant-force springs have been used in previous works for developing stiff structures [35, 36]. Using this method, the tension of the spring and the geometry add together to provide a restoring force for the system undergoing lateral deflection.

6.3.1 Modeling of Passively Wound Orthogonal Beams

Beams in bending due to a lateral load is a well understood phenomena. For a loading in parallel with the strip, the system can be approximated by a simply supported rectangular beam with a force applied as shown in Figure 6.6.

For this loading, the maximum deflection comes at the center of the beam and is

$$\delta = \frac{F_{lat} L^3}{48EI} \tag{6.9}$$

were E is the modulus of elasticity and I is the second moment of area. This is a conservative estimate as the other beam would also contribute a small amount of resistance to bending. The tension in the beams would also contribute to decreasing the deflection. These are both small contributions compared to that provided by the geometry.

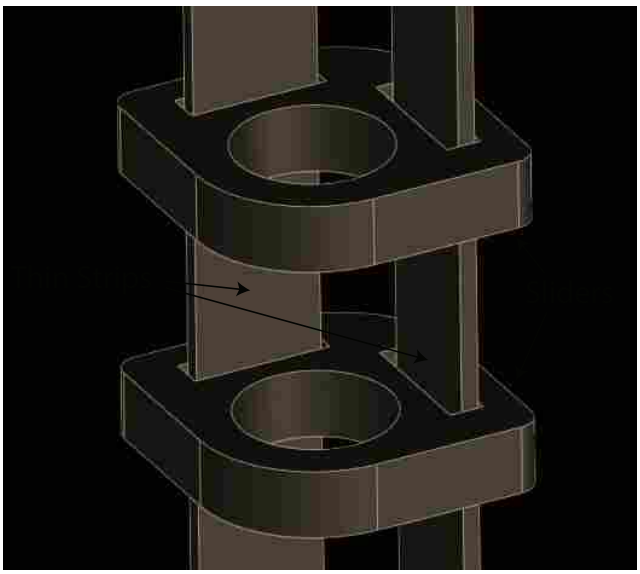

Figure 6.5: Concept of the Orthogonal Beams, the two orthogonal beams are shown with two support sliders. The center holes through the sliders is where the flexible device would pass.

By setting some example parameters, this deflection (Eqn. 6.9) can be compared to the deflection predicted by the Wires in Tension model (Eqn. 6.8). For 10 N of tension in the wires, a fixed length of L=0.5 m for both models, and a 301 stainless steel strip (E=193 GPa, b=0.1524 mm, h=9.40mm), the deflections as F_{lat} increases are shown in Figure 6.7 showing a general trend for the difference between the use of wires or thin strips.

6.4 Physical Validation

As shown in Figure 6.7, geometry of the supporting tension elements can greatly reduce the amount of lateral deflection under a lateral load. For this reason, the orthogonal beams concept was pursued for physical validation.

6.4.1 Prototype

In constructing a prototype, two constant-force springs were used as the strips. The springs used had the same geometry as in the modeling (E=193 GPa, b=0.1524 mm, h=9.40 mm) and exerted just over 1 N each. This force provided for full auto-retraction of the system. Monofilament was used to attach sliders relative to each other and equally space them during actuation. Figure 6.8

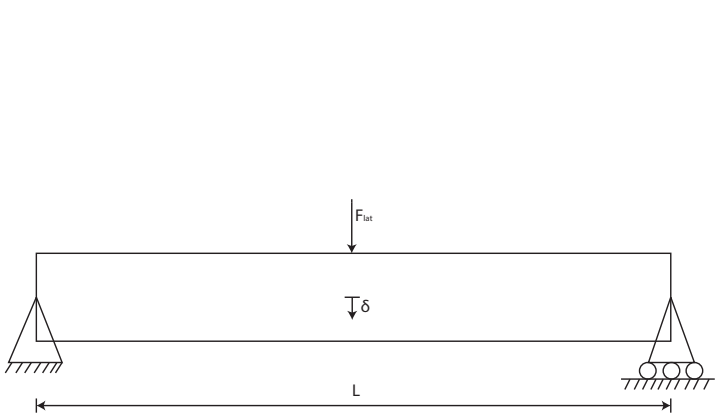

(a) The strip modeled as a simply-supported beam

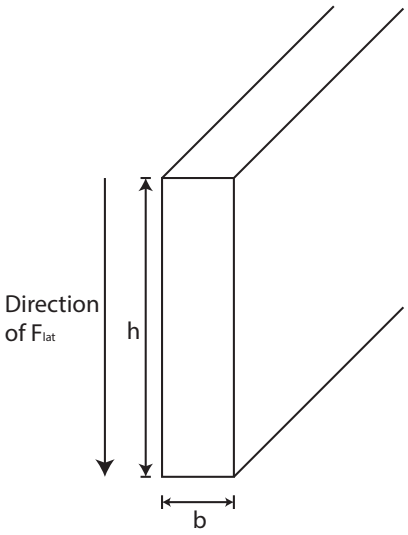

(b) Cross-section of the strip with the force applied parallel to the strip

Figure 6.6: Modeling of the Orthogonal Beams Concept

shows the prototype in the fully compressed and extended states. 6 sliders were used and spacing was designed to mimic that of an existing pantograph system (approximately 50 mm between supports when fully extended). Geometry of the proximal and distal mounts was made to fit an existing robot.

6.4.2 Testing

A 4.5 mm articulating catheter used in robotic surgery was used as a sample device. The catheter was pinned at various lengths and loaded axial until buckling initiated. The following curve fit results in a predicted critical buckling force in newtons from the empirical data. L is measured as the length of the catheter between supports in meters.

$$P_{crit} \approx 0.5532 L^{-1.056} \tag{6.10}$$

This data is shown in Figure 6.9 with the trend of Equ. 6.10 represented as the dashed line.

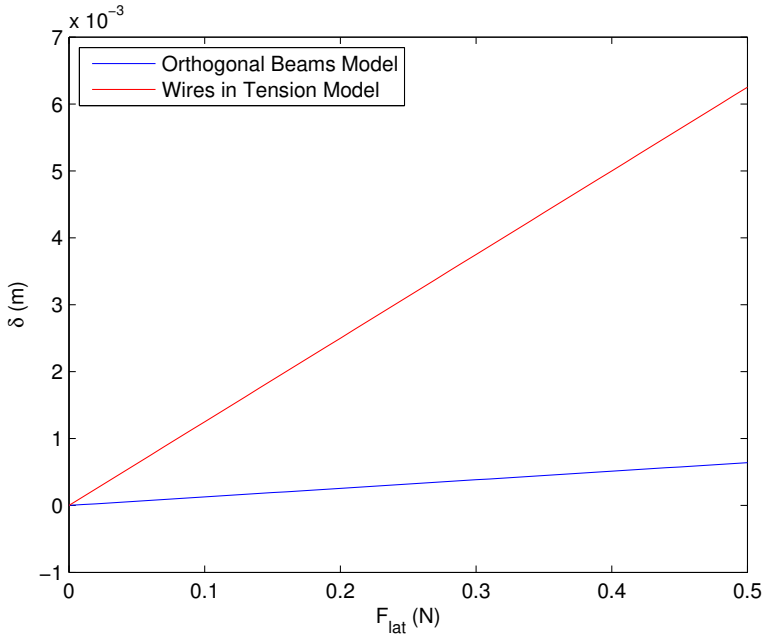

Figure 6.7: Comparison of the force-deflection of the Wires in Tension and the Orthogonal Beams models.

Testing was performed by inserting the catheter into the system and extending the system to a set length. An axial load was applied to the catheter until buckling and a critical buckling load for that length was recorded. These critical loads for each given length are shown in Figure 6.9.

No data is represented for less than 0.15 m for the supported catheter because crushing damage began to initiate in the catheter before buckling failure therefore the test was stopped to avoid damage to the catheter. When buckling initiated, it was always between the supports.

6.5 Discussion

6.5.1 Testing Results

Figure 6.9 shows that the Orthogonal Beams support system can produce a predicable support for a flexible device such as the catheter measured. The support system provides for a fairly constant value for P_{crit}. This is to be expected as the maximum distance between the slider support points is constant. For the tested prototype, the maximum distance was 60 mm. The unsupported catheter for that length is predicted to buckle at just above 10 N, giving the predicted support that

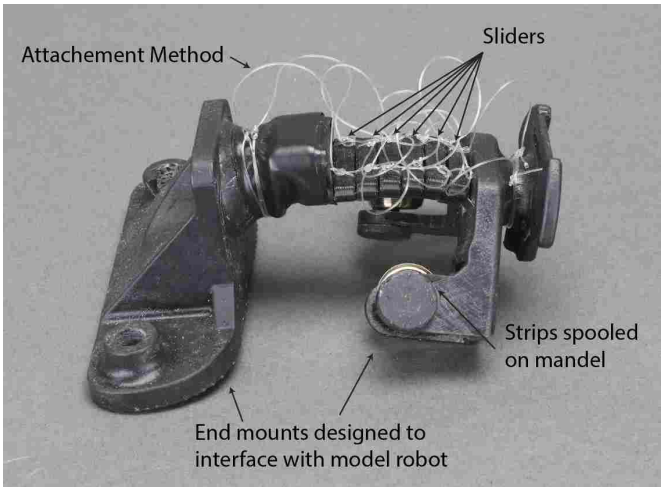

(a) Prototype support system in the fully compressed state

(b) Prototype support system in the fully extended state

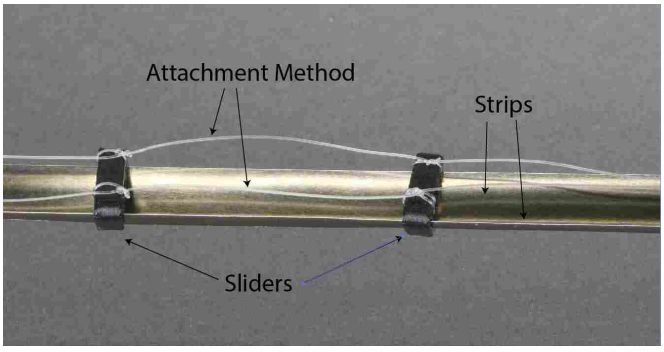

(c) Enlarged image of a section of the fully extended state to demonstrate individual components

Figure 6.8: Orthogonal Beams prototype support system

system would provide, shown by the Predicted Support line in Figure 6.9. The predicted support matches the value for P_{crit} that the support system provides. Therefore the system can be designed for a specified critical buckling load by equating the spacing of the sliders to the length for the same critical load of the unsupported catheter.

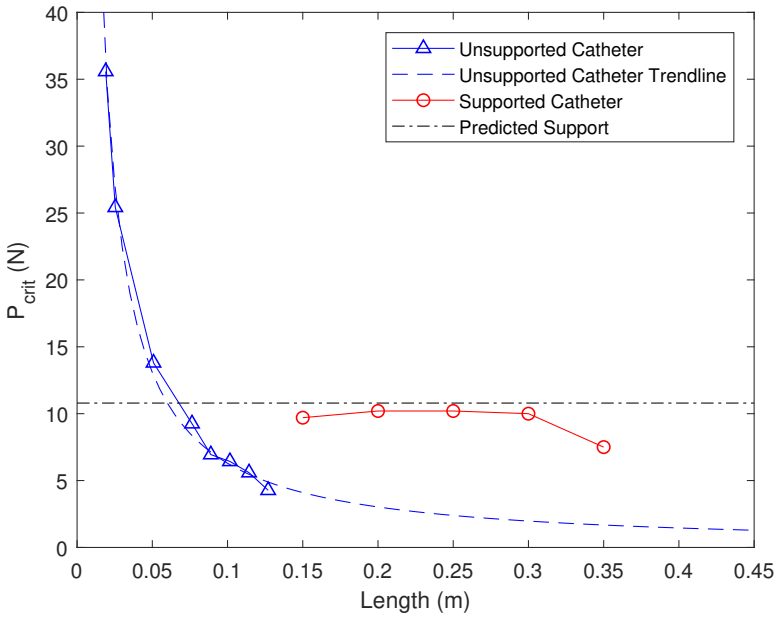

Figure 6.9: Testing data from buckling tests- The predicted support matches the value for P_{crit} that the support system provides.

6.5.2 Enabling Features

The modeling and testing results show that the tension or geometry based systems have highly predictable behavior and can therefore be designed to support a desired device once the device properties are known. They can be designed to mimic the support of a rigid system like a pantograph system. An advantage over the rigid counterpart is the smaller operating volume. Both the Wires in Tension and Orthogonal Beams use sliders as support points and therefore the system does not become wider as the system collapses. Both also decrease in the total part count over a pantograph system.

6.5.3 Other Applications

Changing lengths in cables are commonly used, such as in cranes. This concept could be used to support a flexible device that is needed to be applied at the end of the crane cable such as electrical wiring or collapsible tubing used for carrying fluids such as uncured concrete.

Collapsible booms are commonly used and they find special application in space applications [30–32, 36, 37]. Many of these systems already used constant-force springs or other similar mechanisms to create stiff, self-actuating boom structures. The Orthogonal Beams concept could be used to attach flexible members to these structures or help inspire the use of geometry changes to create stiffer boom structures.

6.6 Conclusion

Using tension in a collapsible system can provide the framework for a support system to which a flexible device can be coupled. As high tension could be undesirable, geometry can be used in the support system to reduce the needed tension while increasing the lateral support. Both systems provide valid and predictable designs for mitigating flexible shaft buckling for devices designed to change the length that needs to be supported, such as medical devices that are unsupported while outside of the body. Both designs also provide advantages over a rigid system in a smaller operating volume and a reduction of part count.

CHAPTER 7. CONCLUSION

In response to the need to support flexible devices in robotic surgery, this research focused on developing an understanding of the principles needed to create anti-buckling support systems. These anti-buckling systems were designed to adapt to changing lengths of device as these devices are inserted into the body. Special focus was made toward reducing the number of parts and the working volume of the support systems. During the development of these principles, additional knowledge was developed and applied that could find application in other areas.

The first support system discussed, the Ori-Guide, showed how origami-inspired engineering can greatly reduce the number of parts while not sacrificing performance. This system provides anti-buckling support through two basic principles: adding tension into a elastic system to increase the lateral stiffness of the system and the addition of discrete support points to reduce the effective length of the flexible member. The pattern developed allows for a large degree of design freedom, making it easily adapted to varying devices and robot dimensional requirements. The pattern integrates bistable and monostable layers together to perform multiple functions in the same sheet material. This could provide the inspiration for other origami-inspired engineering mechanisms as many are designed to perform only one function. One such possible application could be the creation of a tube that both allows flow and has the ability to throttle flow all in the same sheet material.

Working with sheet materials for the Ori-Guide, PET polymer became a primary candidate for the Ori-Guide support system. Further research was conducted to characterize the effects of processing on the material properties, particularly those properties that would lend PET sheets to be a good polymer for this application of origami-inspired engineering. This study helped develop a greater understanding of the workings of this polymer, the effect of cold crystallization, and how the properties can be tailored through thermal processing. There are many other materials that can be used in origami-inspired engineering. Future research into the properties and processing of

other sheet materials could help the field of origami become even more useful to designers and engineers.

Through divergence and iteration during the design process, the Zipper-Tube Reinforcement system was developed. This bore testimony to the influence of good design methods in developing superior products and investigating fields that were originally not obvious. A construction technique was developed and adapted into a system concept that can enable smaller and longer devices than any current support system. This was enabled by the understanding that as the number of discrete support points increase, the buckling strength increases. As that number approaches infinity, or a system is able to provide support along the entire length of the device, the buckling strength greatly increases.

Understanding the underlying physics of buckling failure brought us to focus on counteracting this compressive failure mode by introducing tension into the support system. This was used in both the Ori-Guide and ZTR. Work was also done to minimize the operating volume of the support system. This resulted in the Wires in Tension concept, showing that support can be added to systems through something as small as a thin wire kept taut enough to provide a stiff support structure. Through further thought and investigation, we discovered how geometry can also be used to provide stiff support structures that still operate in a small working volume but provide high stiffness. This was shown by the Orthogonal Beams Support System. The investigation of tension support or geometry could enable engineers and designers to continue to minimize the material used in design and the volume of support structures and systems.

Although research focused on robot-assisted surgery, application of the concepts developed can enable and further engineering and design in multiple areas and disciplines. Geometric changes or the addition of tension systems could find applications in areas where long, thin beams are required such as extendable booms or construction. The addition of support points or supported points along the entire length of devices could find application in the protection of flexible wiring, cabling, or tubing. It could also be used in deployable support structures used for at-risk areas in previously constructed mechanisms and structures.

The contributions of this research include a novel origami pattern that integrates multiple functions into a single pattern developed starting from a basic Kresling pattern. This resulted in a patentable support system. Work done in collaboration with others at the Compliant Mechanisms

Research Group developed a mathmatical model for predicting bistable behavior in the Kresling origami pattern used in the design of the new pattern. This research also provided a deeper understanding of PET films and the use of thermo-processing on their use in origami applications. A novel support system using zipped tubes was created and resulted in a patenable support system. Two more support systems were also developed. These systems developed demonstrated the effectiveness of the application of the additional support points, tension in support systems, changed in geometry, and continuous support in mitigating buckling and all systems proved to mitigate buckling in a thin, flexible device used in robotic surgery.

REFERENCES

[1] Siegel, R. L., Miller, K. D., and Jemal, A. "Cancer statistics, 2018." *CA: A Cancer Journal for Clinicians,* **68**(1), pp. 7–30. 2

[2] Society, A. C. Tests for non-small cell lung cancer `https://www.cancer.org/cancer/non-small-cell-lung-cancer/detection-diagnosis-staging/how-diagnosed.html` Accessed: 2017-11-28. 3

[3] Stahler, G., Romo, E., and WEISS, A., 2012. Anti-buckling mechanisms and methods, Mar. 22 US Patent App. 13/174,563. 4, 37

[4] Howell, L. L., 2001. *Compliant Mechanisms*., 1 ed. John Wiley & Sons, New York, NY. 4, 44

[5] Edmondson, B. J., Bowen, L. A., Grames, C. L., Magleby, S. P., Howell, L. L., and Bateman, T. C., 2013. "Oriceps: Origami-inspired forceps." In *ASME 2013 conference on smart materials, adaptive structures and intelligent systems*, American Society of Mechanical Engineers, pp. V001T01A027–V001T01A027. 4, 11

[6] Dearden, J., Grames, C., Jensen, B. D., Magleby, S. P., and Howell, L. L., 2017. "Inverted l-arm gripper compliant mechanism." *Journal of Medical Devices,* **11**(3), p. 034502. 4, 11

[7] Dearden, J., Grames, C., Orr, J., Jensen, B. D., Magleby, S. P., and Howell, L. L., 2018. "Cylindrical cross-axis flexural pivots." *Precision Engineering,* **51**, pp. 604–613. 4, 11

[8] Butler, J., Morgan, J., Pehrson, N., Tolman, K., Bateman, T., Magleby, S. P., and Howell, L. L., 2016. "Highly compressible origami bellows for harsh environments." In *ASME 2016 International Design Engineering Technical Conferences and Computers and Information in Engineering Conference*. 4

[9] Jianguo, C., Xiaowei, D., Ya, Z., Jian, F., and Yongming, T., 2015. "Bistable behavior of the cylindrical origami structure with kresling pattern." *Journal of Mechanical Design,* **137**(6), p. 061406. 4

[10] Europe, S. S. Buckling restrained braced frames http://www.starseismic.eu, Accessed: 2016-10-26. 5

[11] Kresling, B., Abel, J. F., and Cooke Robert, J., 2008. "Natural twist buckling in shells: From the hawkmoths bellows to the deployable kresling-pattern and cylindrical miuraori." In *Proceedings of the 6th International Conference on Computation of Shell and Spatial Structures, John F. Abel and J. Robert Cooke, eds., Ithaca*. 11, 12, 32

[12] Guest, S. D., and Pellegrino, S., 1994. "The folding of triangulated cylinders, part I: geometric considerations." *Journal of Applied Mechanics,* **61**(4), pp. 773–777. 12

[13] Guest, S., and Pellegrino, S., 1994. "The folding of triangulated cylinders, part II: the folding process." *Journal of Applied Mechanics,* **61**(4), pp. 778–783. 12

[14] Butler, J., Morgan, J., Pehrson, N., Tolman, K., Bateman, T., Magleby, S. P., and Howell, L. L., 2016. "Highly compressible origami bellows for harsh environments." In *ASME 2016 International Design Engineering Technical Conferences and Computers and Information in Engineering Conference*. 12, 23, 32

[15] Cai, J., Deng, X., Zhou, Y., Feng, J., and Tu, Y., 2015. "Bistable behavior of the cylindrical origami structure with kresling pattern." *Journal of Mechanical Design,* **137**(6), p. 061406. 12, 13, 32

[16] Butler, J., Parness, A., Mancini, S., Magleby, S., and Howell, L., 2017. "**IN REVIEW -** Highly compressible origami bellows for microgravity drilling-debris containment." In *AIAA SPACE*. 12, 32

[17] Lv, C., Krishnaraju, D., Konjevod, G., Yu, H., and Jiang, H., 2014. "Origami based mechanical metamaterials." *Scientific reports,* **4**, p. 5979. 23

[18] Johnson, M., Chen, Y., Hovet, S., Xu, S., Wood, B., Ren, H., Tokuda, J., and Tse, Z. T. H., 2017. "Fabricating biomedical origami: a state-of-the-art review." *International journal of computer assisted radiology and surgery,* **12**(11), pp. 2023–2032. 23

[19] Francis, K. C., Rupert, L. T., Lang, R. J., Morgan, D. C., Magleby, S. P., and Howell, L. L., 2014. "From crease pattern to product: Considerations to engineering origami-adapted designs." In *ASME 2014 international design engineering technical conferences and computers and information in engineering conference*, American Society of Mechanical Engineers, pp. V05BT08A030–V05BT08A030. 23

[20] Flores, A., Pieruccini, M., Nöchel, U., Stribeck, N., and Calleja, F. B., 2008. "Recrystallization studies on isotropic cold-crystallized pet: influence of heating rate." *Polymer,* **49**(4), pp. 965–973. 24, 26

[21] Cho, D. H., Yu, W.-R., Youk, J. H., and Yoo, J. H., 2007. "Formation of micro-crystals in poly (ethylene terephthalate) fiber by a short heat treatment and their influence on the mechanical properties." *European polymer journal,* **43**(8), pp. 3562–3572. 24, 25, 26

[22] Karagiannidis, P. G., Stergiou, A. C., and Karayannidis, G. P., 2008. "Study of crystallinity and thermomechanical analysis of annealed poly (ethylene terephthalate) films." *European Polymer Journal,* **44**(5), pp. 1475–1486. 24

[23] Abou-Kandil, A. I., and Windle, A. H., 2007. "The development of microstructure in oriented polyethylene terephthalate (pet) during annealing." *Polymer,* **48**(17), pp. 5069–5079. 24, 25

[24] Martins, C. I., and Cakmak, M., 2007. "Control the strain-induced crystallization of polyethylene terephthalate by temporally varying deformation rates: A mechano-optical study." *Polymer,* **48**(7), pp. 2109–2123. 24, 25

[25] Suzuki, A., and Mochiduki, N., 2001. "Mechanical properties and superstructure of poly (ethylene terephthalate) fibers zone-drawn and zone-annealed by co2 laser heating." *Journal of applied polymer science,* **82**(11), pp. 2775–2783. 25, 26

[26] Chen, W., Lofgren, E., and Jabarin, S., 1998. "Microstructure of amorphous and crystalline poly (ethylene terephthalate)." *Journal of applied polymer science,* **70**(10), pp. 1965–1976. 29, 30

[27] Filipov, E. T., Tachi, T., and Paulino, G. H., 2015. "Origami tubes assembled into stiff, yet reconfigurable structures and metamaterials." *Proceedings of the National Academy of Sciences,* **112**(40), pp. 12321–12326. 32

[28] Zirbel, S. A., Lang, R. J., Thomson, M. W., Sigel, D. A., Walkemeyer, P. E., Trease, B. P., Magleby, S. P., and Howell, L. L., 2013. "Accommodating thickness in origami-based deployable arrays." *Journal of Mechanical Design,* **135**(11), p. 111005. 33

[29] Star seismic europe ltd. buckling restrained braced frames `http://www.starseismic.eu/BRBF_system` Accessed: 2017-04-18. 37

[30] Pellegrino, S., 1995. "Large retractable appendages in spacecraft." *Journal of Spacecraft and Rockets,* **32**(6), pp. 1006–1014. 39, 67

[31] Thomson, M., 1994. "Deployable and retractable telescoping tubular structure development." In *NASA Conference Publication*, NASA, pp. 323–323. 39, 67

[32] Trexler, J. E. C., 1968. Extendible-retractable boom, Jan. 2 US Patent 3,361,377. 39, 67

[33] Coefficient of friction, rolling resistance and aerodynamics `http://www.tribology-abc.com/abc/cof.htm` Accessed: 2017-12-09. 48

[34] Guérinot, A. E., Magleby, S. P., and Howell, L. L., 2004. "Preliminary design concepts for compliant mechanism prosthetic knee joints." *Proceedings of ASME DETC, Salt Lake City*. 54

[35] Seffen, K., You, Z., and Pellegrino, S., 2000. "Folding and deployment of curved tape springs." *International Journal of Mechanical Sciences,* **42**(10), pp. 2055–2073. 61

[36] Murphey, T., Jeon, S., Biskner, A., and Sanford, G., 2010. "Deployable booms and antennas using bi-stable tape-springs.". 61, 67

[37] Costantine, J., Tawk, Y., Christodoulou, C. G., Banik, J., and Lane, S., 2012. "Cubesat deployable antenna using bistable composite tape-springs." *IEEE Antennas and Wireless Propagation Letters,* **11**, pp. 285–288. 67